SAND2000-0762J

(March 14, 2000)

Mechanisms of transition-metal gettering in silicon

S. M. Myers
Sandia National Laboratories, Albuquerque, New Mexico, 87185-1056

M. Seibt and W. Schröter
IV. Physikalisches Institut der Universität Göttingen,
Bunsenstr. 13-15, D-37073 Göttingen, Germany

ABSTRACT

The atomic process, kinetics, and equilibrium thermodynamics underlying the gettering of transition-metal impurities in Si are reviewed from a mechanistic perspective. Methods for mathematical modeling of gettering are reviewed and illustrated. Needs for further research are discussed.

TABLE OF CONTENTS

DISCLAIMER

DISCLAIMER

Portions of this document may be illegible in electronic image products. Images are produced from the best available original document.

I. INTRODUCTION

Transition-metal contamination is ubiquitous in Si devices, being introduced both during wafer growth and in subsequent processing.[1-4] This contamination is frequently detrimental because the transition-metal solutes within Si possess an array of properties that, in combination, can lead to degradation of electronic properties even when the average concentration of the metals is less than one atom per cubic micrometer. Among these properties is a very rapid, interstitial diffusion that allows transport over macroscopic distances during the heat treatments associated with device processing.[5-7] In the extreme case of Cu, recent experimental results indicate a room-temperature diffusion rate sufficient to produce transport over several tenths of a millimeter in 1 hour.[8] Equally important is the small solubility of the metals in Si; typically, solution enthalpies of several electron volts per atom result in vanishingly small concentrations in equilibrium with the metal-silicide phase at temperatures where diffusion is still rapid.[1,5,7] When these two characteristics are combined with the pronounced barriers to metal-silicide nucleation and growth in defect-free regions of the Si lattice,[1,9] there is the possibility of impurity atoms converging from a macroscopic volume to precipitate at an isolated lattice irregularity within a high-quality wafer during cooling. Among the locations where precipitation occurs is the base of gate oxides in metal-oxide-semiconductor (MOS) structures, resulting in electrical breakdown.[1,10] Within the Si matrix, metal atoms in solution and metal-silicide precipitates both introduce deep electronic levels into the bandgap.[1,7,11] These states may reduce minority-carrier lifetimes by orders of magnitude, degrading the performance of devices ranging from large-area solar cells to integrated microelectronics with feature dimensions <1 μm. The importance of these effects is reflected in metal-impurity specifications for starting wafers; for example, a recent projection has Fe tolerances decreasing to $<1\times10^{10}$ atoms/cm^3, or $<2\times10^{-13}$ atomic fraction, in the year 2000, a level which may require new processing methodologies.[2] The 3d elements are of greatest concern because of their prevalence and the degree to which they possess the aforementioned properties, with Fe, Ni and Cu being especially troublesome; however, heavier transition metals such as Au give rise to problems as well.

In controlling the degradation of Si devices by metal impurities, stringent clean-room practices are supplemented by gettering, a class of procedures whereby sinks for the diffusing impurities are introduced into a non-critical region of the wafer. Gettering has proved very effective, and it is employed extensively in microelectronics and photovoltaics. Sinks now in widespread use include SiO_2 precipitates and associated defects within the bulk of Czochralski (CZ) Si wafers that serve as nucleation sites for metal-silicide precipitation (internal gettering);[12,13] substrates with a high concentration of substitutional B acceptors (p^+ substrates) into which charged metal atoms segregate as a result of the Fermi-level offset combined with B-metal pairing;[14-16] deposited Al layers on the back side of the wafer that serve as segregation sinks;[17-19] and a near-surface region of the wafer into which P is diffusing from a deposited or gaseous source, where the effects of a Fermi-level shift and metal-dopant paring are believed to

be augmented by nonequilibrium defect-related processes (phosphorus-diffusion gettering).[9,20,21] The full range of sinks that have been investigated is extensive; in addition to the above it encompasses other electronic dopants,[1,14,22] other second phases in which the metals are soluble such as B-silicide precipitates,[23,24] and a variety of lattice imperfections including point-defect clusters,[25] dislocations,[26] stacking faults,[27] grain boundaries,[28] and cavities where metal-silicide precipitation[29] and atomic trapping[30] occur.

The optimum implementation of gettering differs from one situation to another reflecting a variety of technical and economic considerations. For example, when the device zone occupies only the near-surface region, an oxygen-containing CZ wafer can be heat-treated to introduce SiO_2 precipitates for metal silicide-nucleation throughout the material except within a denuded surface layer extending inward to tens of μm.[31-33] This approach is not applicable to solar cells, however, where long carrier lifetimes over macroscopic thicknesses are needed; then, gettering with strength sufficient to dissolve metal-silicide precipitates in the bulk is desirable, and sinks such as a P-diffusion zone or a layer of Al may be appropriate. Still other circumstances, such as constraints on annealing, the use of Si-on-insulator structures, and the need to reduce impurity concentrations to very low levels, may dictate the use of gettering sinks that are immediately beneath the device zone, possibly with the added property of remaining active at metal concentrations below supersaturation. Under these conditions, sinks such as p^+ substrates, p^+ implanted layers, and implantation-formed cavities may be preferable. Also desirable is the achievement of dual benefits from gettering treatments; examples of this include the combination of P diffusion gettering with the formation of the active p-n junction in solar cells, and the electrical isolation of devices by electronically doped gettering layers beneath the device zone.

Gettering has developed with a strongly operational focus, with empirical observations not infrequently leading to widespread and successful practice in advance of full mechanistic understanding. Partly as a result of this, a specialized nomenclature has emerged that does not always connect transparently and uniquely to underlying physical mechanisms. For example, "internal gettering" and "intrinsic gettering" generally refer to the controlled precipitation of SiO_2 in CZ Si leading to nucleation of metal silicides, while "precipitation gettering" and "relaxation gettering" encompasses all processes based on metal-silicide precipitation. "Segregation gettering" denotes equilibrium enrichment of metal impurities in a portion of the Si wafer or in a deposited back-side layer that results from effects other than metal-silicide precipitation; such effects include atomic pairing with dopants, atomic trapping at defects, locally enhanced solubilities arising from dopant-induced Fermi-level shifts, and solution of the impurity into a precipitated or deposited second phase. Nonequilibrium partitioning due to the interaction between metal impurities and point-defect gradients associated with dopant in-diffusion has been called "dopant-diffusion gettering" and "injection gettering." "Extrinsic

gettering" and "external gettering" usually refer to sinks of any type that are introduced at the back of the wafer.

While the pursuit of performance, reliability, and high production yield at minimum cost is paramount, the importance to these objectives of understanding gettering at a mechanistic and quantitative level has been widely recognized. Such knowledge provides a basis for selection and optimization of established gettering methods, for predicting gettering performance under the increasingly complicated conditions of device processing, and for exploring new approaches. Since advances in these areas are demanded by the evolution of Si device technology, a substantial body of fundamental research has addressed the physical processes that underlie gettering. The results of this research are the principal subject of the present article.

In the sections that follow we review current fundamental understanding of the metal binding reactions that underlie present and prospective methods of gettering and describe the mathematical treatment of these processes. Particular attention will be given to the 3d elements from Ti to Cu and to the heavier elements in the Ni and Cu columns of the periodic table, all of which exhibit the rapid interstitial diffusion that promotes detrimental effects in devices. Rather than exhaustively referencing the extensive literature on gettering that spans three decades and includes more than 1800 papers, we selectively cite findings that bear upon the consideration of underlying processes. We begin by summarizing in Section II certain relevant properties of the transition metals in solution in the Si lattice. Then, in Section III, a series of subsections describe the fundamental types of gettering reaction. The discussion ranges from atomic processes to reaction kinetics and equilibrium thermodynamics and their relationship to observed phenomenology. Section IV discusses mechanism-based modeling, with examples chosen to illustrate a range of considerations bearing on device processing. Conclusions are presented in Section V.

II. PROPERTIES OF THE TRANSITION-METAL SOLUTES

The transition-metal impurities in Si that are the subject of gettering reside at least partially on interstitial solution sites, enabling the rapid diffusion that magnifies their detrimental effects. Substitutional lattice sites are also occupied, to a degree that varies greatly among the metals. In intrinsic Si, the 3d elements from Ti to Cu and the 4d metal Pd are believed to be predominantly interstitial, while Zn, Pt, and Au reside preferentially but not exclusively on substitutional sites. These metal solutes are further characterized by multiple charge states and associated deep levels in the bandgap, giving rise to the reduction of carrier lifetime discussed in the introduction. The known charge states range from –2 to +2, with the neutral and +1 states predominating for interstitial atoms in intrinsic Si and negative charge states being mostly associated with substitutional atoms. There is now a substantial body of information concerning

the energies of the variously charged interstitial and substitutional states. Recent reviews are available,[1,7,14,22] and herein we cite selected results as they bear upon the discussion of gettering mechanisms. The multiple charge states persist to elevated temperatures, and as a result the Fermi level can strongly affect the solubility of a metal and its partitioning between interstitial and substitutional sites during gettering treatments.

The solution state is both the starting point and the thermodynamic reference for the gettering reactions to be considered, so that, for purposes of the discussion, it is desirable to avoid the complexities described above. To this end, we make two stipulations. First, the reference state for the specification of sink binding strengths is always the interstitial component of solution, independent of the relative occupancies of the interstitial and solution sites. This choice is convenient since it is the mobile interstitial atoms that actually undergo the gettering reactions. The reference condition is further simplified by specifying that the metals are gettered from a region of the Si where the Fermi level is at its intrinsic position. This choice has the effect of establishing a single dominant charge state, usually either neutral, as for elements from Ti to Co, or +1 as for Cu. Since gettering takes place primarily at elevated temperatures where Si is close to intrinsic unless heavily doped, the difference between the above reference state and the device region of a wafer can often be neglected.

The rapid diffusion of the transition metals is believed to take place predominantly by the movement of atoms from one interstice to another without the involvement of point defects. This mechanism is made possible by the relatively small size of the metal atom combined with the openness of the diamond lattice, whose tetrahedral interstitial site provides the same available hard-sphere volume as the substitutional site. As a result, some of the metals, notably Co, Ni, Cu, and Pd, are among the most mobile of all solutes in Si. When substitutional as well as interstitial solution sites are occupied, as for Zn, Pt, and Au, the transport still proceeds primarily through interstitial migration; while movement between neighboring substitutional sites mediated by thermal point defects is expected to take place, this process is much slower. As has been discussed in detail for Au and Pt,[6,34] transfers between the interstitial and substitutional components of solution are believed to occur through the reversible kick-out mechanism whereby an interstitial metal atom, M_i, displaces a Si host atom from its lattice site creating a substitutional metal atom, M_S, and a self-interstitial, I:

$$M_i \leftrightarrow M_S + I \,. \tag{1}$$

A further contribution to the transfer may arise from the Frank-Turnbull mechanism, where the interstitial metal combines with a vacancy, V, according to the equation

$$M_i + V \leftrightarrow M_S \,. \tag{2}$$

The reaction of Eq. (1a) is endothermic in the forward direction while Eq. (2) is exothermic. Since these reactions introduce a coupling between the diffusion of interstitial metal atoms, the diffusion flux of point defects, and the rate of conversion between interstitial and substitutional metal atoms, the metal transport is complicated and is related to the interstitial-metal diffusion coefficient in a convoluted manner. (This problem has nevertheless been formulated and solved using numerical methods; see, *e.g.*, Refs. 35-37.) One consequence is that, while the interstitial-atom diffusion coefficients for the predominantly interstitial transition metals have been experimentally quantified with some confidence, in the case of metals such as Zn, Pt, and Au that have large substitutional components, quantitative description of the transport is less advanced.

Representative experimentally determined diffusion coefficients for predominantly interstitial transition metals in Si are shown in Fig. 1, with the metal charge state being indicated where known.[8,38-40] (Comprehensive reviews of metal diffusion rates in Si appear elsewhere.[5,7]) All of these results are believed to reflect the behavior of intrinsic Si except the segment for $Fe^{(+)}$, which is applicable to p-type material. Included for comparison are the diffusivities of Si and B atoms,[41,42] which are substitutional in Si and undergo much slower, point-defect-assisted diffusion. This figure illustrates the rapidity of diffusion by the interstitial mechanism, and it also exhibits the large increase in diffusion rate on going from left to right in the periodic table. While incompletely understood, this variation is believed to arise in substantial part from the decrease in the atomic size of the solute as the number of valence electrons increases, which reduces the elastic-strain contribution to the migration enthalpy.[43] Much less is known about the influence of metal charge state on the diffusion, and available information is not entirely consistent; in the case of Fe, for example, different signs have been reported for the change between the neutral and +1 state.[39,44] Generally speaking, however, the reported charge-state dependencies are small compared to the variation between elements and are not sufficient to influence substantively the considerations of gettering herein; the offset between the nearby segments for $Fe^{(0)}$ and $Fe^{(+)}$ in the figure is typical. The horizontal dashed lines in Fig. 1 indicate approximate threshold diffusivities for, respectively, atomic redistribution on the scale of a few atomic spacings, diffusion through the ~10 μm device layer of a modern microelectronics device, and diffusion from the front side of a wafer to the back side. Noting the intersections of the latter two lines with the diffusivity results reveals an important advantage of "proximity gettering," wherein sinks are located immediately beneath the device zone, as compared to back-side gettering.

The transport of transition-metal impurities over macroscopic distances is abetted by the pronounced inhibition of metal-silicide precipitation in the undefected Si lattice, even under conditions of great supersaturation. Important factors contributing to this property are believed to include the activation barrier to nucleation of the phase, the interfacial energy, and the elastic and plastic deformations required to accommodate reaction volume changes.[1,9] The precipitation behavior is illustrated by transmission-electron-microscopy (TEM) results for Ni in

Si,[45] a case where the volume change is relatively small, – 0.02 Si atomic volumes per $NiSi_2$ formula unit at room temperature. When float-zone Si saturated with Ni at temperatures between 850 and 1050°C was rapidly quenched, precipitation during or after cooling to room temperature produced a particle density of only 4×10^{10} cm^{-3}, or one precipitate in 25 μm^3. The resultant particles were coherent {111} platelets up to 1 μm in diameter but only 0.63 nm thick corresponding to two {111} layers of $NiSi_2$; an example is shown in the high-resolution TEM image of Fig. 2. The platelets are bounded by a dislocation and associated with a stacking fault in the Si matrix in order to accommodate the atomic structure of the {111} precipitate-matrix interfaces. All Ni atoms in such platelets belong to the interfaces and have a sevenfold coordination compared to eightfold in bulk $NiSi_2$, revealing the metastability of these initially formed precipitates. Rough estimates of the energy associated with the {111} interfaces and the bounding dislocation indicate extremely large nucleation barriers and considerable driving forces for precipitate ripening, primarily through thickening of the platelets.[45] In fact, after low-temperature annealing (below 320°C), *internal ripening* of precipitates has been observed which results in platelets with a typical thickness of several nm while leaving the precipitate density unaffected[11]. Conventional precipitate coarsening leading to a reduction in the number of particles (Ostwald ripening) has been observed for temperatures above 500°C , again accommodated primarily by platelet thickening. The thermal evolution is represented in Fig. 3, which shows particle number density and thickness as a function of anneal temperature. Notably, the volume of Si host per $NiSi_2$ precipitate ultimately reached ~3000 μm^3. More generally, rapid quenching of low-defect Si causes the metal impurities with the highest mobilities, including Co, Ni, Cu, and Pd, to undergo low-density precipitation within the bulk and form silicide particles on the surface with an adjacent depleted zone.[1,9] Less rapidly diffusing species, including the 3d elements from Ti to Fe and Pt and Au, may remain in solution for extended periods. The precipitation behavior differs markedly in the presence of defects, which strongly promote silicide nucleation and growth as discussed in Section III.A.

III. GETTERING MECHANISMS

We consider five mechanistically distinct types of binding reaction that have proved effective for gettering of transition-metal impurities. Discussed first is the precipitation of metal silicides at deliberately introduced nucleation sites. In this case, the residual concentration in solution in the Si phase asymptotically approaches a value corresponding to thermodynamic equilibrium within the two-constituent, two-phase system. The equilibrium compositions of the two phases depend only upon temperature from the Gibbs phase rule, with the metal concentration in the Si being the solid solubility. The next mechanism also involves a second phase, but now one formed by a third elemental species, with the transition metal being a dilute constituent. An example is Al-Si liquid on the back side of the wafer. In this situation, and in the limit of small metal concentrations, equilibrium is characterized by a direct proportionality

between the transition-metal concentrations in the two phases. The final solution concentration in the Si is thus not restricted by a fixed solubility, and the gettering mechanism operates at all impurity concentrations, in contrast to the first mechanism. The third mechanism is atomic trapping at Si-lattice defects without second-phase formation. This is another process characterized in the limit of small metal concentrations by a proportionality between the occupancies of solution and gettered states, and the gettering again remains active for solution concentrations below the solubility. While such trapping should in principal occur at a wide variety of imperfections, detailed, quantitative observations have so far been limited to cavities. The final two types of gettering process involve interactions of the transition metals with a high concentration of charged electronic dopants within the gettering zone. We first consider the case where the dopant is immobile in an otherwise perfect lattice. Then, the binding arises from the combination of two effects: first, the Fermi-level shift caused by the dopant lowers the energy of charged metal atoms in the gettering region; and, second, there is a largely electrostatic pairing reaction between charged dopant atoms and oppositely charged transition-metal atoms. A well studied example of this is the gettering of Fe within B-doped Si. Lastly, we discuss phosphorus-diffusion gettering, which occurs when P diffuses into a Si wafer at high concentration. This is a particularly strong but still incompletely understood gettering process where the above equilibrium dopant effects are believed to be augmented by nonequilibrium phenomena involving point-defect fluxes.

A. Metal-silicide precipitation

The precipitation of transition-metal silicides from interstitial solution is an effective and widely used method of removing metal impurities from the device region of a wafer. Procedures based on this effect are often termed precipitation gettering, and also relaxation gettering because they involve the relaxation of supersaturated solutions toward equilibrium. The success of the approach is due to two properties of the Si-metal system: first, the already discussed inhibition of homogeneous nucleation, which means that the second-phase formation can be mostly restricted to deliberately introduced nucleation centers; and, second, the strong thermodynamic driving forces for the phase transition, which allow the solution concentration to be reduced to small values. The minimum impurity concentration theoretically achievable by such gettering is equal to the solid solubility at the temperature of the last processing anneal where there is sufficient solute mobility for diffusion to the sinks. In practice, the precipitated phase observed after such anneals usually conforms to the equilibrium phase diagram,[1,9] although the initial stages of $NiSi_2$ formation can involve very thin platelets with deficient coordination[45] as already discussed, and a metastable silicide of Au has been observed.[46] (In this regard, precipitation from solution contrasts with the reactions of deposited metal films on the external surface of Si, where intermediate, metal-rich silicides often occur.[47]) Consequently, the solution

concentration is expected ultimately to approach the equilibrium solubility during isothermal annealing.

Largely because of their importance to gettering, transition-metal solubilities in Si have been extensively studied.[1,5,7] For convenience and to facilitate extrapolation, experimental solubility results are generally parameterized using equations based on approximate solution models. Equating the chemical potentials of metal atoms interstitially dissolved in Si and metal atoms in the solid silicide phase gives in the limit of small solution concentration

$$[M_i]^{sol} = \exp\left(\frac{\Delta S^o_{sil}}{k} - \frac{\Delta H_{sil}}{kT}\right) \tag{3a}$$

where $[M_i]^{sol}$ is the atomic fraction of metal in solution in equilibrium with the silicide, ΔS^o_{sil} is the concentration-independent part of the entropy change caused by transferring one metal atom from the silicide to interstitial solution, and ΔH_{sil} is the corresponding change in enthalpy. Here use has been made of the fact that the density of tetrahedral interstitial solution sites is equal to the density of Si atoms. The entropy and enthalpy parameters are taken to be independent of temperature. In accord with our stipulation in Section II, the reference solution state for ΔS^o_{sil} and ΔH_{sil} is always intrinsic Si. This means that, for charged metal atoms within electronically doped material, the argument of the exponential in Eq. (3a) has an additional term:

$$\left[M_i^{(\sigma)}\right]^{sol} = \exp\left(\frac{\Delta S^o_{sil}}{k} - \frac{\Delta H_{sil}}{kT} - \frac{\sigma\left(E_F - E_F^i\right)}{kT}\right) \tag{3b}$$

where σ is the integer charge state, E_F the Fermi level, and E_F^i the Fermi level in intrinsic Si.

Above the eutectic temperature of the Si-metal system, the phase in equilibrium with the dilute solid solution is a liquid with temperature-dependent composition, and as a result the thermodynamics are more complicated. An idealized model of the liquid found to provide an adequate representation of experimental results[5,7] leads to the relation

$$[M_i]^{sol} = [M_{liq}] \exp\left(\frac{\Delta S^o_{liq} - \Delta S^{fus}_M}{k} - \frac{\Delta H_{liq} - \Delta H^{fus}_M}{kT}\right) \tag{4}$$

where $[M_{liq}]$ is the atomic fraction of metal in the liquid, ΔS^o_{liq} is the concentration-independent part of the entropy change caused by transferring one metal atom from the pure metal to interstitial solution in Si, ΔH_{liq} is the change in enthalpy resulting from the same atom transfer, and ΔS^{fus}_M and ΔH^{fus}_M are the atomic entropy and enthalpy of fusion of the metal. The equilibrium composition of the liquid can be evaluated at each temperature from the phase diagram, or it can be approximately calculated as discussed elsewhere.[5]

In the case of metals that predominantly occupy substitutional sites in intrinsic Si, including Zn, Pt, and Au, the interstitial solubility is generally not well known. It is then customary to specify the substitutional solubility, $[M_S]^{sol}$, or the total solubility, which are more accessible experimentally. For internal consistency, however, we will continue to take the interstitial solution as the reference state. The relationship between the interstitial and substitutional solubilities is given by

$$\frac{[M_i]^{sol}}{[M_S]^{sol}} = \exp\left(\frac{\Delta S^o_{sub}}{k} - \frac{\Delta H_{sub}}{kT}\right) \tag{5}$$

where ΔS^o_{sub} and ΔH_{sub} are, respectively, the change in concentration-independent entropy and the change in enthalpy caused by moving one metal atom from substitutional solution to interstitial solution without introducing a Si vacancy. We note that there is a general absence of quantitative experimental information on ΔS^o_{sub} and ΔH_{sub}, and that this introduces some indeterminacy into the modeling of gettering for the predominantly substitutional metals.

The solubilities of representative, predominantly interstitial solutes from the first transition series are shown in Fig. 4 for intrinsic Si below the eutectic temperature.[5,48] The solid lines represent experimental data as fitted by Eq. (3a), while the dashed lines are extrapolations. Additional information is provided by Table I, which lists values of the parameters in Eqs. (3)-(5) for intrinsic Si at temperatures relevant to gettering. It should be emphasized that these values are intended to provide a convenient representation of experimental solubility data, and that they correspond to true thermodynamic enthalpies and entropies only to the degree that the simplified treatment of the solubilities is accurate. In the case of the primarily substitutional metals, the tabulated quantities serve to specify the substitutional solubility, which is what has been measured. (For a more comprehensive recent review, see Ref. 7.) The results in Fig. 4 serve to make the point that gettering by metal-silicide precipitation, while potent, cannot be regarded as totally effective or irreversible. Processing temperatures for Si devices extend to ~1000°C, where, for example, the solubility of Fe exceeds 10^{14} atoms/cm^3 and those of Cu and Ni are much higher still; in comparison, impurity concentrations as small as 10^{10} atoms/cm^3 may be of concern. This means that the gettering anneal must take place at some temperature well below 1000°C that allows the required reduction in impurity concentration while simultaneously providing the mobility necessary to reach the gettering sinks. Furthermore, any subsequent heat treatment at a higher temperature can reintroduce the impurity into solution and so remove the benefits. In practice, gettering by metal-silicide precipitation is often accomplished during cooling after the final processing anneal.

Consideration of Fig. 4 in conjunction with Fig. 1 shows more specifically the interplay of diffusivity and solubility in determining the optimum gettering anneal, and reveals in

particular the significance of the distance from the device region to the gettering sinks. In the case of Fe, for example, a gettering anneal with a duration of 1000 s must take place at ~1000°C or above in order for sinks at the back-side of the wafer to be effective, but the residual concentration of 4×10^{14} atoms/cm^3 at this temperature is often unacceptable. If, instead, the sinks are located immediately beneath the device zone at a diffusion distance of only ~10 μm in order to achieve proximity gettering, then a temperature of ~300°C is sufficient, and here the equilibrium solubility of Fe is negligible. Such a small diffusion distance is not possible, however, if the active device region extends throughout the wafer, as in a photovoltaic device or photodetector. Furthermore, if back-side gettering is used, the introduced sinks must compete with defect-related silicide-nucleation sites throughout the wafer, where precipitation is undesirable. Hence, alternative gettering methods that are capable of reducing the concentration to below the solubility and so dissolving unwanted silicide precipitates may be preferable for bulk devices. Mechanisms considered in the following subsections satisfy this criterion.

Factors of the kind discussed above make it desirable to model the time evolution of the gettering. A widely used approach in such calculations is to assume that the interstitial solution concentration immediately adjacent to a gettering site is equal to the equilibrium solubility of the metal. This means that the kinetics are governed entirely by diffusion, with no inhibition due to the precipitation reaction itself. Although, departures from this idealized condition are not inconsequential, as discussed below, currently available information does not support a more elaborate treatment. With the boundary condition thus established, the diffusion problem can be addressed. While a wide range of gettering configurations arise, they can usually be adequately treated in one of two ways. First, when the gettering zone contains sinks at a density sufficiently high in relation to the distance to the device region, the gettering zone can be regarded as one continuous sink with the solution-concentration boundary condition applied at its margin. This simplification is often appropriate, for example, in the case of gettering at the back side of the wafer, or gettering within an ion-implanted layer proximate to the device region. When, however, the sinks are widely separated from each other, it may be necessary to treat them individually. This condition typically holds when the nucleation sites are SiO_2 precipitates distributed through the bulk of a CZ-Si wafer and extending to within a few micrometers of the surface (internal gettering). In such cases, a more accurate but still tractable formulation is obtained by taking the silicide-precipitate sinks to be spherical with a single effective radius, R_{sil}. As shown elsewhere,[58] when R_{sil} is much smaller than the distance between sinks, the concentration profile near a particular sink quickly approaches the steady-state solution of the diffusion equation for an isolated sphere in an infinite medium. Within this steady-state approximation, the number of metal atoms moving to each sink per unit time is $4\pi R_{sil}N_{Si}D_i\{[M_i] - [M_i]^{sol}\}$, where N_{Si} is the atomic density of Si, D_i is the diffusion coefficient of the interstitial metal atoms, and $[M_i]$ is the solution atomic fraction averaged over a volume containing multiple sinks. For a given number density of silicide-precipitate sinks, N_{sil}, one then obtains

$$\frac{\partial [M_{sil}]_{Si}}{\partial t} = 4\pi R_{sil} N_{sil} D_i \{[M_i] - [M_i]^{sol}\} = \frac{1}{\tau}\{[M_i] - [M_i]^{sol}\} \quad (6)$$

where $[M_{sil}]_{Si}$ represents a volume-averaged atomic fraction of metal atoms occupying silicide precipitates within the Si host. More specifically, $[M_{sil}]_{Si}$ is the number of metal atoms divided by the total number of atoms within a volume containing multiple precipitates; this quantity is distinct from the much larger atomic fraction of metal atoms within the silicide phase itself, which we denote herein as $[M_{sil}]$. The quantity $\tau \equiv (4\pi R_{sil} N_{sil} D_i\}^{-1}$ is a characteristic time for the approach to local equilibrium within the gettering zone. Equation (6) can be incorporated into a transport-reaction formalism describing the overall evolution of the system, as discussed in Section IV. In the case of a uniform system at constant temperature with no time dependence of R_{sil} and no competing reactions to affect $[M_i]$, the difference from equilibrium is predicted to decay as $\exp(-t/\tau)$. The departure from Eq. (6) when the sink volume fraction becomes large has been discussed elsewhere.[59,60]

In reality, the metal concentration adjacent to a gettering sink can differ significantly from the thermodynamic solid solubility, being additionally influenced by the kinetics of the precipitation reaction; only when local equilibration at the sink is rapid in relation to the diffusion of impurities to the sink is the solubility boundary condition underlying Eq. (6) strictly appropriate. Precipitation begins with an agglomeration of metal atoms at the nucleation site giving rise to the silicide phase, and this step may have a significant activation barrier. Then, during subsequent growth, interfacial energy and the strain energy arising from the reaction volume change cause the chemical potential of the metal to be greater than that of an unconstrained bulk silicide. The strong influence of interfacial energy is exhibited in the already discussed case of $NiSi_2$ precipitation,[11,45] where volume-strain effects are small due to the minimal lattice mismatch. The growth of coherent $NiSi_2$ platelets of high aspect ratio, such as that shown in Fig. 2, evidences a kinetic activation barrier for the formation of incoherent interfaces. Further, the pronounced ripening and reduction of aspect ratio caused by subsequent annealing reflect the consequential energies associated with both coherent and incoherent interfaces.

The volume change associated with precipitation varies widely among the metal silicides and can be substantial;[1,61] for example, the formation of $FeSi_2$ from solution produces a change of -0.11 Si atomic volumes per metal atom at room temperature, while the change is only -0.02 for $NiSi_2$, and reaches the large positive value of $+0.5$ for Cu_3Si. The effect of the resultant strain upon precipitation is particularly evident for the case of Cu, where precipitation of Cu_3Si is accompanied by the formation of strain-relieving dislocations that then serve as sites for further particle nucleation.[62] This process results in precipitate-dislocation colonies, such as that shown in the TEM micrographs of Fig. 5.

It has been hypothesized that metal-silicide precipitation can be significantly inhibited by electrostatic repulsion when the interstitial metal solute and the precipitate are both positively charged.[63] Deep-level electronic states associated with $NiSi_2$ and Cu_3Si particles in Si have been investigated[11,64] using deep-level transient spectroscopy (DLTS),[65] revealing localized or band-like character.[66] In the case of Cu, the band-like silicide is believed to go from positive to neutral as the Fermi level rises into the upper region of the bandgap, while the interstitial solute atom remains positively charged throughout. This change with increasing Fermi level was found to correlate with an increased tendency for Cu to precipitate within the Si matrix instead of migrating to the external surface, prompting the inference of precipitation inhibition by electrostatic repulsion. This proposed kinetic effect is in addition to the increase in thermodynamic driving force for precipitation caused by an increase in the Fermi energy as represented in Eq. (5b).

The influence of the above precipitation-inhibiting effects on gettering rate is made greater by the very rapid diffusion of the transition metals in Si. As a result of the fast transport, precipitation may occur at relatively low temperatures where the influence of activation barriers is greater and where thermal self-diffusion is too slow to contribute to the accommodation of local volume changes. Additionally, reaction-rate bottlenecks are more consequential when the diffusion to the reaction site is rapid.

The implication of the above considerations for gettering in devices is that the rate of impurity accumulation in the sinks may be smaller than predicted by a model based on diffusion-limited kinetics, affecting both the time dependence of the residual solution concentration and the way in which the metal-silicide phase is partitioned among nucleation centers within the wafer. The likelihood of such effects being important rises with the metal diffusion coefficient. The diffusivity increases by orders of magnitude on going from left to right in the periodic table, as seen in Fig. 1; hence, for example, a reaction bottleneck is far more probable for Cu than for Ti. Evidence of reaction-related retardation has been reported for some conditions of Fe gettering, as discussed below. In contrast, the asymptotically approached value of the residual solution concentration is not expected to differ significantly from the equilibrium solubility, and to our knowledge no such departure has been observed experimentally.

Microstructural studies have illuminated the processes of metal-silicide precipitation for a range of metal impurities and silicide-nucleating defects. Although understanding remains incomplete, and is insufficiently quantitative to revise the solubility boundary condition leading to Eq. (9), such work has yielded important qualitative insights that will now be discussed. We begin by noting that the unoxidized free surface of Si should be among the most favorable sites for metal-silicide precipitation, since this surface provides reduced steric hindrance during nucleation, diminished interfacial energies during growth, and ready accommodation of volume changes. Consistent with this view, ion-implanted Cu and Au in Si were observed by TEM to

migrate from the implanted layer, which contained a high density of extended defects, to a nearby layer containing pre-existing cavities, where precipitation occurred in the cavity open volumes.[29,67] (Such three-dimensional precipitation in cavities is distinct from sub-monolayer chemisorption on the walls, which is characterized by different energetics and kinetics and will be considered as a defect-trapping mechanism in Section III.C.) The external surface of Si is also a sink despite the presence of SiO_2, as shown by surface precipitation of the more mobile transition metals Co, Ni, Cu, and Pd during cooling.[1,68]

The Si-SiO_2 interface is again a site of metal-silicide formation during gettering by a bulk dispersion of SiO_2 particles (internal gettering). The kinetics of the metal precipitation in this technologically important case have been investigated experimentally for Fe.[12,13,69,70] The isothermal decay of the solution concentration was found to be consistent with the exponential time dependence predicated by Eq. (9), as seen from the results plotted in Fig. 6.[12] Moreover, at lower temperatures where the driving force for precipitation is relatively large, experimentally determined time constants were semiquantitatively consistent with values of $(4\pi R_{ppt}\,[ppt]_N\,D_i)^{-1}$ independently estimated from the microstructure, and the activation energy of the rate was close to that of D_i. When, however, high particle densities were combined with higher temperatures where the driving force for precipitation is reduced and the diffusion more rapid, the observed precipitation rate was slower than predicted by more than an order of magnitude; this presumably means that the reaction rate was not controlled entirely by diffusion to the SiO_2 particles. Selected results exhibiting this effect are shown in Fig. 7.[13] To account for such behavior, it was hypothesized that prompt nucleation of the metal-silicide phase occurs only at some locations on the Si-SiO_2 interface. In another study, relatively large, faceted SiO_2 particles were reported to getter Fe more effectively than smaller, spherical, more numerous oxide precipitates during slow cooling from 1050°C; yet, during isothermal annealing at 190°C, the smaller particles gettered more rapidly and in accord with diffusion-limited kinetics.[69] Again in this case, one apparently has evidence for the influence of reaction kinetics at the more elevated temperature.

A range of microstructural studies encompassing Fe, Ni, Co, Cu, and Pd in Si show an association of metal silicide particles with dislocations, indicating that these extended defects support the precipitation process.[45,62,71-74] In addition to promoting nucleation, dislocations are believed to facilitate relief of the strain caused by the precipitation volume change; proposed mechanisms for the latter effect include dislocation punching and the absorption of ejected Si interstitials through dislocation climb. Evidence for such relaxation is especially compelling in the already discussed case of Cu, where the Cu_3Si particles are observed to form in colonies accompanied by the generation of numerous dislocations, as seen in Fig. 5. Full dislocations have been found to getter Cu more strongly than the Frank partials bounding stacking faults.[71]

Grain boundaries and stacking faults have also been observed to promote metal-silicide precipitation from supersaturated solution, to a degree that depends upon the character of the discontinuity. In a study of Si bicrystals containing Ni or Cu, the gettering effectiveness of three types of twin boundary was assessed by measuring the thickness of the adjacent metal-depleted region after annealing.[28] The extent of gettering varied greatly and, as noted by the investigators, exhibited a positive correlation with the theoretically estimated interfacial energy. Separately, TEM analysis of $NiSi_2$ precipitation within a deposited layer of polycrystalline Si showed the silicide particles to be associated predominately with small-angle grain boundaries, leading the investigators to suggest that grain-boundary dislocations play a role in this case.[75] In yet another study, large stacking faults bounded by Frank partial dislocations were found to getter Fe predominantly to the dislocations during slow cooling, indicating a lesser affinity for the fault plane; with rapid cooling, however, where the driving force for precipitation was greater, precipitation occurred also on the fault plane.[27]

Ion implantation into Si for purposes of gettering has been examined for a wide range of implantation conditions and ions, and some degree of gettering has been observed virtually without exception. As reported in many papers over three decades, H, He, B, C, O, N, F, Ne, P, Ar, Ge, As, Kr, and Si self-ions have been implanted at energies from tens of keV to the MeV range and at doses from $\sim 10^{14}$ to 10^{17} atoms/cm^2, with the gettered species including Fe, Co, Ni, Cu, Pd, Ag, Pt, and Au. (See, *e.g.*, Refs. 10,15,24,29,30,37,67,71,76-82.) Detailed mechanistic interpretation has often proved challenging in these studies because of the complexity of the implanted microstructure, which typically contains dense agglomerations of dislocations, stacking faults, vacancy complexes, and self-interstitial clusters with the added possibility of impurity-defect centers, solid precipitates, gas bubbles, voids, and amorphous layers, all evolving during the gettering anneal.[83,84] From the foregoing discussion, however, it seems highly probable that nucleation of metal-silicide precipitates at the numerous lattice imperfections plays an important role in implantation gettering, in addition to several other mechanisms that will be considered in the following subsections. It should nevertheless be noted that experimental confirmation of this by such relatively conclusive methods as direct TEM observation of the silicide particles,[71] or demonstration that the residual solution concentration after rapid quenching is consistent with the thermodynamic solid solubility at the gettering temperature,[82] has only rarely been reported for the technologically relevant regime of low impurity levels. Silicide precipitation has frequently been observed, however, in cases where the transition metals were ion implanted to concentrations above about $\sim 10^{-3}$ atomic percent in conjunction with heat treatments.[85-88] Finally, it has been proposed that the metal solution concentration in the vicinity of metal-silicide precipitates within an implanted layer at elevated temperatures can remain either much smaller or much larger than the equilibrium solubility for extended periods as a result of the interplay between point defects and the precipitation volume change.[89] Effects of this kind were invoked to account for dissolution of Cu_3Si particles at a

rate much smaller than predicted from consideration of the Cu solubility and diffusivity at the anneal temperature of 780°C.

In summary, gettering by precipitation of metal silicides, or relaxation gettering, is an effective and widely used means for removing metal impurities from the device region of wafers. This mechanism has been implemented in a variety of ways, the most extensively used methods being internal gettering at SiO_2 particles and back-side gettering within a deposited layer of polycrystalline Si; other investigated sinks include back-side mechanical damage, ion damage either at the back of the wafer or immediately beneath the device region, and cavities in these two locations. An important limitation of precipitation gettering is that the residual solution concentration cannot be reduced below the solid solubility of the impurity. As a result, the gettering cannot reverse precipitation within the device region. Moreover, precipitation gettering usually must be carried out at temperatures $<<1000$°C, where the reduced mobility of the metal may unacceptably limit the range of the sinks. While extensive data is available on the relevant solubilities, important gaps remain, most notably for the interstitial solubilities of metals with a large substitutional solution component. The microstructural processes and kinetics of silicide formation have been elucidated only at a qualitative level. As a result, quantitative modeling of the time evolution of the gettering is currently limited to the approximation of diffusion-limited kinetics embodied in Eq. (6).

B. Segregation into second phases

We now consider the gettering of transition metals by previously formed second phases that comprise Si and some third elemental species with the gettered impurity incorporated as a dilute constituent. Such processes are among those referred to as segregation gettering, distinguishing them from the relaxation gettering treated in the preceding subsection. Two gettering phases of this type have been investigated, liquid or solid Al-Si on the back side of the wafer,[17-19,90-94] and B-Si precipitates within the Si matrix.[23,24,95-97] An important difference from the precipitation of transition-metal silicides is that equilibration of the system no longer uniquely determines the compositions of the two phases, since the third elemental constituent gives rise to an additional degree of freedom in accord with the Gibbs phase rule. Instead, the volumes of the two phases and the total number of metal-impurity atoms are the quantities determined by experimental conditions, and the transition-metal concentrations in the two phases adjust within these constraints to equalize chemical potentials, as detailed below. A second difference is that the kinetics of the gettering reaction are expected to have much less influence on gettering rate than in the case of metal-silicide precipitation, since now the reaction does not involve nucleation or significant changes in volume and interfacial area. Hence, modeling based on diffusion-limited kinetics should generally be more quantitative.

Assuming that there is only one type of transition-metal site in the second phase and that it is far from saturation, equating the transition-metal chemical potentials in the two phases gives

$$[M_i]^{sps} = [M_{sp}] \exp\left(\frac{\Delta S^o_{sps}}{k} - \frac{\Delta H_{sps}}{kT}\right) = [M_{sp}] \frac{1}{K_{sps}} \tag{7}$$

where $[M_i]^{sps}$ is the equilibrium atomic fraction of transition-metal interstitials in the Si phase resulting from the second-phase segregation, $[M_{sp}]$ is the atomic fraction of the transition metal in the second phase, ΔS^o_{sps} is the concentration-independent part of the entropy change when one transition-metal atom moves from the second phase to solution in the Si, ΔH_{sps} is the corresponding change in enthalpy, and K_{sps} is the segregation coefficient. An important implication is that the ratio of the equilibrium metal concentrations in the two phases depends only on temperature. As a result, the gettering reduces the solution concentration in the Si phase by a factor that does not depend on the magnitude of the concentration, so that the gettering does not cease below the solid solubility as happens in the case of metal-silicide precipitation.

In modeling the time evolution of the gettering, which is expected to be limited by diffusion in the Si phase as already indicated, the appropriate boundary condition at the margin of the second phase is simply $[M_i] = [M_i]^{sps}$ with the latter quantity given by Eq. (7). When the second phase is present as a dispersion of discrete precipitates within the Si matrix rather than a continuous layer, considerations similar to those leading to Eq. (6) give

$$\frac{\partial [M_{Si}]_{Si}}{\partial t} = \frac{1}{\tau} \{[M_i] - [M_i]^{sps}\} \tag{8}$$

where $[M_{sp}]_{Si}$ is the volume-averaged atomic fraction of precipitated metal in the Si and $\tau \equiv \{4\pi R_{ppt} [ppt]_N D_i\}^{-1}$. Equation (8) can be incorporated into a diffusion-reaction formalism describing the overall evolution of the system.

When Al is deposited onto a Si wafer and the specimen annealed above the eutectic temperature of 577°C, a liquid Al-Si alloy forms. This liquid is Al-rich over most of the temperature range relevant to gettering, the Si content being 12 at.% at the eutectic and about 56 at.% at 1000°C.[98] The molten layer is in contact with the Si lattice as a result of the SiO_2 layer being reduced by the Al, so that transition-metal atoms are expected to move readily between the two phases and rapidly approach the local equilibrium given by Eq. (7) in the vicinity of the interface. The transition metals have substantial solubilities in liquid Al, generally ranging from several at.% upward,[98] while their solubilities in crystalline Si at comparable temperatures are orders of magnitude less, as illustrated in Fig. 4. This suggests that the gettering from Si into liquid Al-Si should be strong. The two binary phase diagrams do not allow quantitative prediction of the segregation coefficient K_{sps} in Eq. (7), however, in light of

the non-negligible reaction enthalpies for formation of transition-metal silicides from their elemental constituents.[47,99]

In experimental studies related to photovoltaics, a number of workers have shown that deposition of Al and subsequent annealing at temperatures above ~600°C improves device properties in a manner consistent with removal of transition-metal impurities. (See, *e.g.*, Refs. 90-94.) Two other investigations measured the reduction in the concentration of a specific impurity caused by the gettering, one by detecting Co through radioactive-tracer methods,[18] and the other by using DLTS to observe Fe.[19] In both instances, the investigators determined lower bounds on the segregation coefficient rather than its value. In the case of Co, the gettering was carried out at 820°C with the result $K_{sps} > 1 \times 10^4$. The experiments on Fe utilized gettering temperatures from 750 to 950°C and yielded values of K_{sps} extending to $\sim 1 \times 10^6$. The greatest segregation of Fe was found at the highest temperature, an effect suggested by the authors to arise from incomplete equilibration.

In the case of the latter two experiments, the identification of the underlying mechanism as segregation into the Al-Si phase is reinforced by several considerations. Precipitation of transition-metal silicides, discussed in the preceding subsection, can presumably be ruled out, since the residual concentrations in the Si phase were far below the solid solubility and precautions were taken to avoid significant gettering during cooling after the anneal. Another mechanism likely to be active to some degree is binding between the transition metal and substitutional Al that has diffused some small distance into the Si lattice from the molten layer. Aluminum is a shallow acceptor and hence negatively charged at the temperatures of interest, so that the dopant-associated gettering of positively charged metal atoms to be discussed in Section III.D is expected to occur. It is difficult to account for so strong an effect at such elevated temperatures by this mechanism, however. Moreover, in the case of Co, the Mössbauer spectrum of gettered ^{57}Co atoms was measured after cooling to room temperature, and comparison was made with reference data from a separately prepared Al-Si-Co liquid that was similarly quenched from the melt; the results support the presence of the gettered Co within the previously liquid Al-Si layer.[18]

Gettering by segregation into a deposited Al layer can also take place below the eutectic temperature of 577°C. There is again a large difference in transition-metal solubilities between the two phases suggestive of strong driving forces, and, for highly mobile species such as Cu and Ni, the mobility is sufficient for diffusion through the thickness of a wafer. Experimental results exhibiting such gettering were reported for Cu, where an Al film dissolved Cu_3Si phase from the opposite side of the wafer.[17]

Summarizing, the occurrence and effectiveness of gettering by deposited Al layers has been demonstrated, and the evidence for an equilibrium segregation mechanism appears strong.

Deficiencies in current knowledge include the small number of metal impurities for which the segregation effect has been specifically and definitively observed, and the absence of experimental values for the equilibrium segregation coefficient. We also note that Sn and Pb layers have been proposed as potentially superior alternatives to Al; in addition to forming low-melting eutectics with Si, the former elements are isoelectronic with Si and relatively insoluble, making unwanted electrical doping less of a concern.[100] To date, however, experimental examination of these alternatives has not been reported.

Another second phase giving rise to strong segregation gettering is a silicide of approximate composition B_3Si that precipitates when Si is implanted with B to supersaturation and then annealed.[95,96] A phase-contrast TEM image of one such particle is shown in Fig. 8. The pronounced granularity of the particle image at all specimen orientations, combined with the absence of a diffraction pattern, led to the conclusion that the precipitated phase lacks long-range structural order. This disordered state remains even after annealing at 1200°C for 24 hours. The concentration of B in the Si lattice near the B-Si particles was found to be close to the solubility reported for crystalline B_3Si, implying a near coincidence of B chemical potentials. On the basis of this and other considerations, it was proposed that the observed disordered phase is an advanced precursor to crystalline B_3Si, with similar local coordination and bonding but lacking the full long-range order of the complex, icosahedron-containing rhombohedral structure. (It should be noted that other, contrasting conclusions have been reported concerning the nature of the B-Si precipitates.[101] High-resolution TEM images of Si that was implanted with B and then annealed showed the pattern of the Si lattice image continuing unbroken over the position of the precipitates, leading the investigators to infer that the particles were crystalline and coherent with the host lattice.)

Iron, Co, Cu and Au were found by SIMS, RBS, and analytical TEM to segregate to the above B-Si phase, with simultaneous dissolution of the silicides of the metals in a separate layer.[24,95] Such behavior indicates a gettering mechanism other than metal-silicide precipitation. This interpretation was reinforced by Mössbauer spectroscopy of gettered ^{57}Co, whose quadrupole-split spectrum differed qualitatively from that observed for $^{57}CoSi_2$, but conformed closely to the spectrum of ^{57}Co ion-implanted into bulk crystalline B_3Si.[97] Further supporting evidence came from detailed studies of Fe gettering, where the equilibrium number of gettered metal atoms was determined as a function of the atomic fraction of interstitial Fe in the Si phase, $[Fe_i]$, the latter quantity being measured by DLTS.[24] At both 900 and 1000°C, a proportionality was maintained between the gettered and solution components of the Fe for $[Fe_i]$ extending as much as two orders of magnitude below the solubility, in accord with Eq. (7). (Gettering by the substitutional component of B within the Si lattice was appreciable but much smaller at such elevated temperatures, as shown by control experiments where the B was implanted below supersaturation. This is consistent with findings discussed in Section III.D.)

The segregation coefficient for Fe obtained from these experiments is shown as a function of temperature in Fig. 9, where the enrichment relative to the Si phase is seen to extend above 10^6.

Strong gettering of Fe closely similar to that shown in Fig. 9 was reported for deposited layers of Si that were doped with high concentrations of B during growth, but only when the B concentration exceeded ~10^{20} atoms/cm^3, close to the B solubility at the annealing temperatures of the study.[23] The activation energy associated with the segregation coefficient was found to be 2.1 eV, as compared to the value of 2.27 eV seen in Fig. 9. The investigators concluded that the observed gettering was due to an electrically inactive form of the B, whose specific nature was not determined in that study. It seems plausible that the gettering mechanism is the same as that discussed above for the supersaturation implants of B. Consistent with this interpretation are separate observations of B precipitation within highly doped wafers at comparable temperatures.[102]

Several issues related to gettering by B-Si particles remain unresolved. Among these are, under what conditions the disordered and crystalline forms of B-Si precipitate in Si doped during growth, and whether the structurally disordered form is required for the strong gettering discussed above. The most extreme of the annealing treatments used in Ref. 102, 240 hours at 1100°C, was reported to produce μm-size, faceted precipitates with an electron diffraction pattern ascribed to icosihexahedra-containing orthorhombic SiB_6; this compound has recently been identified as the true equilibrium phase,[103] rather than B_3Si as concluded earlier.[98] At 900°C, however, much smaller particles formed whose structural state was not established. Another unresolved issue is the nature and density of the metal-atom sites within the gettering B-Si phase; one can at present say only that the site density is as great as the largest observed concentration of gettered atoms within the phase, ~2 at.% in the case of Cu.

C. Atomic trapping by defects

In Section III.A, we discussed the demonstrated effectiveness of a variety of defects in nucleating transition-metal silicide phases. A number of these imperfections are also expected to be sinks for single metal atoms as a consequence of their being associated with open regions in the lattice and Si atoms that are incompletely coordinated and hence reactive. Here we refer to such solute-defect reactions not involving second-phase formation as trapping, and we consider them as a distinct type of mechanism. Demonstrating the absence of precipitation at defect sinks may be difficult on the basis of TEM alone, since a second phase can comprise a small number of atoms. The difference in gettering behavior is profound, however, since metal-silicide precipitation does not saturate but ceases when the solution concentration of the metal reaches the solid solubility, whereas, as discussed below, trapping is a saturable process that remains active at all concentrations. In the following, we begin by using an idealized physical model to

illustrate the characteristics and mathematical description of gettering by trapping. Then we discuss two specific trapping mechanisms, chemisorption on the walls of cavities, and binding to defects of believed vacancy character that are produced by MeV ion implantation at a depth of about one-half the ion range. These are cases where a degree of success has been achieved in differentiating atomic trapping from metal-silicide precipitation.

For purposes of modeling, we consider a dispersion of identical traps within the Si lattice, each capable of binding a single metal atom. It is further assumed that the trapping reaction is reversible and has no significant activation barrier beyond that associated with lattice diffusion. In equilibrium, one then has

$$[M_i]^t = \left(\frac{[M_t]}{[t]-[M_t]}\right)\exp\left(\frac{\Delta S_t^o}{k}-\frac{\Delta H_t}{kT}\right) \tag{9}$$

where $[M_i]^t$ is the equilibrium atomic fraction of metal atoms in interstitial solution in equilibrium with the traps, $[M_t]$ is the atomic fraction of trapped atoms, $[t]$ is the atomic fraction of traps, ΔH_t is the change in the enthalpy of the system caused by transferring one metal atom from trap to solution, and ΔS_t^o is the corresponding change in the concentration-independent entropy. It is evident from Eq. (9) that, when the traps are far from saturation so that $[M_t] << [t]$, there is a proportionality between the solution and trapped concentrations that persists to arbitrarily small impurity levels. As a result, this mechanism is classified as segregation gettering. The analogous equation for metal-silicide precipitation, or relaxation gettering, given in Eq. (3) contains no concentration dependence on the right-hand side, so that gettering ceases when the solution concentration reaches the solid solubility. Trap saturation is manifested in Eq. (9) as the divergence of the prefactor on the right-hand side when $[M_t]$ approaches $[t]$.

The time evolution of the above gettering can be treated as a competition between diffusion-limited trapping at unoccupied sites, whose atomic fraction is $[t] - [M_t]$, and activated release from the occupied traps present at atomic fraction $[M_t]$. This gives for the time derivative of the trapped atomic fraction

$$\frac{\partial[M_t]}{\partial t} = 4\pi R_t N_{Si} D_i \left([M_i]([t]-[M_t])-[M_t]\exp\left(\frac{\Delta S_t^o}{k}-\frac{\Delta H_t}{kT}\right)\right) \tag{10}$$

where R_t is the effective radius of reaction for the trap. Equation (10) reduces to the form for diffusion-controlled reaction when all traps are unoccupied, and the asymptotically approached equilibrium condition conforms to Eq. (9). This treatment can be elaborated in a variety of ways to accommodate more complicated situations. One example is the cavity trapping discussed below, where the trap sites reside on the surfaces of spherical sinks rather than being individually dispersed. In this case equilibrium is again described by Eq. (9) provided that the traps act

independently; however, the diffusion prefactor in Eq. (10) should be replaced by $4\pi R_t N_{Si} D_i / n_t$, where R_t is now the effective radius of the combined sink and n_t is the number of trap sites per sink.

Numerous workers have examined the gettering of metals by cavities in Si, with the investigated species including Fe, Co, Ni, Cu, Ag, Pt, and Au. (See, *e.g.*, Refs. 24,29,30,37,67,79,81,104-115.) These sinks are formed by ion-implanting He or H at room temperature to concentrations above about 1 at.% and then annealing, usually in the temperature range 700-1200°C. Pressurized bubbles form during the implantation, and this is followed during annealing by out-diffusion of the gas, by ripening of the open volumes to sizes as large as ~10 nm accompanied by faceting, and by extensive annihilation of other implantation-related defects. Trapping, as distinct from the formation of three-dimensional metal silicides discussed in Section II.A, is believed to occur through a chemisorption-like reaction on the cavity walls. One type of evidence for this effect is exemplified in Fig. 10, which shows the RBS-measured accumulation of Cu within a cavity-containing layer accompanied by dissolution of equilibrium-phase Cu_3Si on the opposite side of the wafer during annealing at 600°C.[110] The fact of Cu redistribution from the silicide-containing layer to the cavities tends by itself to support a gettering mechanism other than metal-silicide precipitation. From Eq. (3), there should be no concentration gradient to drive Cu diffusion from one Cu_3Si-containing layer to another during the anneal; silicide-to-silicide redistribution could arise only from second-order influences not included in Eq. (3), such as interfacial and strain energies and self-interstitial supersaturation arising from the process of Cu_3Si formation. Moreover, precipitation of additional Cu from solution during cooling should not be an important factor in this experiment where the amount of redistribution between layers is relatively large. A second feature supporting a chemisorption mechanism is the saturation of gettering at an areal density of about 5×10^{15} Cu/cm^2, which is close to the value estimated for monolayer coverage of the cavity walls using TEM images, $(4.7\pm0.7)\times10^{15}$ Cu/cm^2. Finally, high-resolution TEM images of the cavities after gettering showed no indication of metal-silicide formation, as seen from the inset in Fig. 10.

The chemisorption of metal atoms on cavity walls is in general a complex process involving multiple types of binding site, surface reconstructions, and interactions between neighboring metal atoms at higher coverages. (See, *e.g.*, the discussion of Au on the (111) surface of Si in Ref. 116.) As a first approximation, however, experimental data on cavity gettering have been analyzed under the assumption that there is a unique binding site whose properties are unaffected by occupation of neighboring sites, so that Eqs. (9) and (10) are applicable.[30,37,110] Such analysis was employed to extract a temperature-dependent binding free energy, ΔG_t, defined in terms of the parameters of Eqs. (9) and (10) as

$$\Delta G_t \equiv \Delta H_t - T\Delta S_t^o . \qquad (11)$$

Two experimental approaches were used to obtain ΔG_t. In one of these, a cavity layer was allowed to come into equilibrium with a separate layer containing a large excess of equilibrium metal-silicide phase, thereby stabilizing the solution concentration $[M_i]$ at the known solid solubility $[M_i]^{sol}$; then, RBS or SIMS was employed to evaluate the trapped concentration $[M_t]$, and TEM was used to estimate the concentration of trap sites [t], thereby allowing ΔG_t to be extracted by substituting into Eq. (10). In the case of Fe, the expected value of the solution concentration in equilibrium with the metal silicide was verified by DLTS. This equilibrium approach was used successfully for Fe and Co.[30]

The same method was applied to Cu and Au,[37,110] but in these cases the value of ΔG_t was sufficiently large relative to the stability of the silicide to drive the chemisorption nearly to saturation, so that the numerator $[t] - [M_t]$ in Eq. (9) could not be experimentally quantified; hence, only a lower bound on ΔG_t was obtained. To achieve quantification for Cu and Au, the rate of metal redistribution from an initially saturated cavity layer to a second, initially unoccupied cavity layer was measured.[37,110] The gradient in solution concentration driving the interlayer redistribution arises from the dependence of the solution concentration adjacent to a cavity, $[M_i]^t$, upon the occupancy of that cavity, $[M_t]$, as expressed in Eq. (9); consequently, the redistribution continues until the fractional occupation of trap sites is the same in the two layers. (In the case of Au at cavity-wall coverages of ~1 monolayer, the interlayer redistribution did not continue to the point of equal partitioning, a departure interpreted in terms of ordered-island formation rather than the random-site chemisorption on which Eq. (9) is based.[37]) Using an independently evaluated diffusion coefficient, a numerical solution of the diffusion problem was fitted to the redistribution data by adjusting ΔG_t. The results from both types of analysis are summarized in Fig. 11, where ΔG_t is plotted as a function of temperature for the four metals. The temperature ranges of the data were considered insufficient to support the evaluation of ΔH_t and ΔS_t^o separately.

The results in Fig. 11 indicate a strong gettering reaction at the cavity walls. For example, when $\Delta G_t = 1.4$ eV, at the lower extreme of the plotted values, and the temperature is 900°C, the fractional occupation of the traps exceeds that of solution sites by a factor of $\sim 10^6$ for impurity levels below saturation. It has been hypothesized that the stronger trapping of the monovalent metals Cu and Au relative to the multivalent Fe and Co, which is opposite to the trend in metal-silicide formation energies, arises to some degree from the difficulty in accommodating high bonding coordination on the surface.[30] A more complete experimental characterization and theoretical analysis can be expected to alter some particulars of the above description, revealing, for instance, multiple binding energies and ordered-island surface states of the kind observed in ultrahigh-vacuum (UHV) studies of external surfaces.[116] Already, Mössbauer spectroscopy of gettered ^{57}Co has provided evidence for more than one type of bound state;[81] indirect evidence has emerged for Au-island formation on cavity walls at higher occupancies;[37] UHV studies of Cu gettered from internal Cu_3Si precipitates to well

characterized external surfaces[117] have shown that the (111) surface, which predominates on cavity walls,[118,119] is a more effective sink than the (100) surface; and observation of the gettering of Au to competing large and small cavities has prompted the conclusion that the smaller sinks are more effective for the same internal surface area.[114] Nevertheless, it seems probable that the semiquantitative inferences arising from Fig. 11 will remain.

Ion implantation at relatively high, MeV energies is being explored as a means to introduce defect-related gettering sites beneath the device region of wafers. In certain of these studies,[25,82,120] gettering of Fe and Cu has been observed to take place not only at the ion end-of-range (R_p) where dislocation defects are observed by TEM after annealing, but also at a depth of about ~$R_p/2$ where no defects are evident from microscopy. The so-called "$R_p/2$ gettering" is rendered ineffective by diffusion of oxygen to the region, whereas the end-of-range gettering is not. A further, profound difference is that the sinks at $R_p/2$, when not passivated by O, were found to reduce the nearby solution concentration of Fe to a level two orders of magnitude below the solid solubility for an anneal temperature of 800°C, as measured by DLTS after rapid quenching.[82] In contrast, the end-of-range defects reduced the concentration only to the solubility, consistent with metal-silicide precipitation. The strong gettering at $R_p/2$ has been ascribed to atomic trapping at vacancy clusters on the basis of several considerations: first, Monte-Carlo simulations of ion stopping within Si show that the differing depth distributions of collision-produced vacancies and interstitials should result in a net excess of vacancies at depths less than the ion range;[25,121] second, depth profiling of the implantation defects by positron-annihilation analysis with a variable-energy beam showed a concentration of open-volume defects at the appropriate depth;[25] third, the binding strength associated with interstitial-metal trapping at vacancy clusters is expected to be substantial as a result of strain relief and possible passivation of dangling orbitals; and, finally there is arguably a parallel with the more readily characterized trapping at cavities. It should be noted, however, that this interpretation has been questioned by investigators who observed interstitial-type dislocation loops at the gettering depth using TEM.[122]

D. Interaction with electronic dopants

Most transition-metal solutes in Si are charged for some range of Fermi energies,[1,7] and this property can be exploited for gettering through manipulation of the depth profile of electronic dopants. Two physical effects underlie such gettering: first, a charged metal atom and a dopant atom with opposite charge may form a bound pair, with the binding being due largely to electrostatic attraction but also influenced by other effects such as strain; and, second, when the level of electronic doping is sufficient to shift the Fermi level, the energy of the charged metal atom is reduced still further. As a result of the simultaneous operation of these effects, metal impurities segregate from an intrinsic or lightly doped region of a wafer into a highly doped

gettering zone. This zone may be a thin layer beneath the device region, such as that formed by ion implantation of the dopant, or it may comprise the bulk of the wafer with the device layer being grown epitaxially on top. The most thoroughly investigated example is the gettering of Fe in highly B-doped Si. We will use this case to illustrate the characteristics and mathematical description of such gettering and then conclude the discussion with more general considerations.

Interstitial Fe occupies the neutral and +1 charge states in Si. In equilibrium, the atomic fractions of these states are related by

$$\frac{\left[M_i^{(+)}\right]}{\left[M_i^{(0)}\right]} = \exp\left(\frac{G_M^{(0/+)} - E_F}{kT}\right) \tag{12}$$

where E_F is the electron chemical potential or Fermi energy, and $G_M^{(0/+)}$ is the metal donor level including ionization enthalpy and entropy terms. Studies using DLTS have shown that, for Fe, $G_M^{(0/+)}$ lies about 0.39 eV above the valence-band edge, E_V, in the vicinity of room temperature.[7,22] Results for the solubility of Fe in highly B-doped Si provide evidence that $G_M^{(0/+)} - E_V$ varies little with temperature up to about 700 or 800°C, but decreases substantially at higher temperatures.[14,16] The pairing between the charged interstitial metal atom, $M_i^{(+)}$, and the charged substitutional acceptor, $A_S^{(-)}$, is expected to obey an equilibrium relation of the form

$$\frac{[M_iA_S]N_{Si}}{\left[M_i^{(+)}\right]\left[A_S^{(-)}\right]} = \exp\left(-\frac{\Delta S^o_{MA}}{k} + \frac{\Delta H_{MA}}{kT}\right) \tag{13}$$

reflecting a balance between the pairing and dissociation reactions, where ΔH_{MA} is the enthalpy change and ΔS^o_{MA} the change in the concentration-independent entropy arising from the dissociation of one pair. For Fe in B-doped Si, experimental measurements of the three populations near room temperature and below are well described by Eq. (13) with $\Delta S^o_{MA}/k = 0.70$ and $\Delta H_{MA} = 0.65$ eV.[123,124]

The equilibrium partitioning of Fe between the B-doped gettering region and the remainder of the wafer can be calculated by applying Eqs. (12) and (13) to both regions and using the fact that the equilibrium concentration of the neutral metal, $[M_i^{(0)}]$, is independent of location. (The B-Fe pair has a donor level 0.1 eV above the valence-band edge whose influence will be neglected here.[22]) In calculating the Fermi energy for use in Eq. (12), it is often adequate to assume electrical neutrality at every location, neglecting the space charge associated with spatial variations in dopant concentration. With this simplification, standard formulae giving the charges associated with dopants, conduction electrons, and holes as a function of E_F can be

applied and E_F adjusted to achieve the neutrality The departure from neutrality caused by a change in dopant concentration extends for a distance on the order of

$$L \sim \sqrt{\frac{\varepsilon_0 K_S \Delta E_F}{q^2 N_D}} \tag{14}$$

from the step, where ε_0 is the permittivity of vacuum, K_S the dielectric constant of the semiconductor, ΔE_F the corresponding change in the position of the Fermi level in the band gap, q the elementary charge, and N_D the atomic density of the charged dopant. Consequently, depth dependencies on a scale $\lesssim L$ should in principle be treated by a more elaborate procedure involving solution of Poisson's equation. (See, *e.g.*, Refs. 125,126.) For a modest doping level of $N_D = 1\times10^{15}$ atoms/cm^3 in Si and $\Delta E_F = 1$ eV, $L \sim 1$ μm. Hereinafter, the simplification of charge neutrality will be used.

Examples of the behavior predicted for Fe in B-doped Si are shown in Fig. 12. Here the calculated ratio of total Fe concentration in the B-doped region to that in the adjoining intrinsic Si, or the segregation coefficient, is shown as a function of temperature for three B concentrations. Also included are dashed lines representing the enrichment due solely to the Fermi-level shift in the absence of the pairing reaction. These computational results serve to illustrate significant properties of gettering by electronic doping. One such feature is that large segregation coefficients can be realized, but primarily at relatively low temperatures. In view of the diffusion rates shown in Fig. 1, this implies that the diffusion distance between the gettering sinks and the device region should be microscopic. Such an approach has been followed in practice, either through epitaxial growth of Si on highly doped substrates[127-129] or by ion-implanting B immediately beneath the device region.[15,130] Another noteworthy feature of Fig. 12 is that the segregation coefficient increases approximately as the square of B concentration at lower temperatures, reflecting the fact that the B concentration affects E_F in Eq. (12) as well as appearing explicitly in Eq. (13).

In treating the time evolution of gettering by electrical dopants, it is generally a good approximation to assume that the pairing reactions and the changes of metal charge state occur instantaneously, so that Eqs. (12) and (13) are satisfied at all times and locations. The description of the time dependence is then accomplished by introducing a third equation that gives the atomic flux due to migration of interstitial metal atoms:

$$\vec{J}_M = -N_{Si} D_i^{(0)} \nabla\left[M_i^{(0)}\right] - N_{Si} D_i^{(+)} \nabla\left[M_i^{(+)}\right] - N_{Si} D_i^{(+)} \left[M_i^{(+)}\right]\left(\frac{1}{kT}\right)\nabla(E_F - E_V) \,. \tag{15}$$

The first two terms on the right-hand side take account of random-walk diffusion, with provision being made for a dependence of the diffusion coefficient D_i upon charge state, while the last term describes the drift of charged atoms in electric fields associated with dopant gradients.

The theoretical description of Fe behavior in B-doped Si based on Eqs. (12), (13), and (15) has been compared with a variety of experimental information and found to yield quantitative, internally consistent agreement for temperatures up to about 800°C. In particular, the pairing reaction was studied by DLTS for temperatures up to about 200°C and found to conform to Eq. (13).[123,124] Separately, the enhancement of the total solubility of Fe in Si caused by a high concentration of B, 1.5×10^{19} atoms/cm^3, was measured at temperatures from 800 to 1100°C, and good agreement with Eqs. (12) and (13) was found for 800°C; at higher temperatures the enhancement was progressively less than calculated, an effect provisionally ascribed to a reduction in $G_M^{(0/+)} - E_V$.[16] Finally, the time-dependence of gettering was examined in an experiment where Fe moved from bulk solution to a B-implanted layer during cooling; the depth profile of gettered Fe was measured by SIMS, and the depth profile in solution was obtained by DLTS combined with sputter erosion, providing a detailed characterization. The results agree quantitatively with predictions based on Eqs. (12), (13), and (15) using independently evaluated parameters.[15]

More generally, such gettering by highly p-doped layers is expected to occur for metals that become positively charged when the Fermi level approaches the valence-band edge, and this criterion is satisfied for all of the transition-metal solutes whose electronic properties have been investigated. Cases where large segregation coefficients have actually been observed include Mn, Fe, and Co in B-doped Si.[14,16] Equations (12), (13), and (15), with extensions as needed to take account of higher charge states, should serve to describe such gettering when parameter values are known. Extensive information is available on the electronic levels of the transition-metal solutes, as summarized elsewhere.[1,7] Knowledge of the binding enthalpies for pair formation is more limited. Experimentally determined values reviewed elsewhere[14,22,131,132] are generally comparable to what is calculated for a simple electrostatic interaction between point charges at neighboring substitutional and tetrahedral interstitial sites, 0.52 eV,[133] , but the departures are not insignificant; for example, 0.5 eV was found for B-Mn, 0.65 eV for B-Fe, and 0.61 eV for B-Cu.

Many of the transition-metal solutes also have negative charge states,[7] so that high donor concentrations can produce gettering analogous to that discussed above for p-type doping. In Si doped with 1×10^{20} P/cm^3, the lattice concentrations of Fe and Co in equilibrium with the respective metal silicides at 700°C were observed to increase by more than three orders of magnitude from intrinsic Si; moreover, in the case of Fe, the enhancement was greater by a factor of 20 than observed for B doping at nearly the same concentration.[14] In the case of Au, a P concentration of 4×10^{19} atoms/cm^3 increased the solubility at 800°C by a factor of about 15.[134]

As was found for p-type doping, the segregation coefficient decreases rapidly with increasing temperature. Most of the negative metal charge states are believed to be associated with atoms on substitutional lattice sites, so that the occupancy of such sites increases as the Fermi level rises. Among the consequences of this enhanced substitutionality is a reduction in the effective diffusion coefficient of the metal, as observed for Fe and Co.[14] The oppositely charged donor and metal atoms are expected to undergo pairing, and, indeed, Mössbauer spectroscopy of ^{57}Co in P-doped Si revealed coexisting entities identified as substitutional Co and P-Co pairs. Analysis of the temperature dependence of the concentration ratio [CoP]/[Co_S] yielded a binding enthalpy of 1.5 eV.[14]

Mathematical modeling of gettering in n-type layers is generally more complicated than in p-type because the metals occupy both interstitial and substitutional sites. As a result, the metal states that must be taken into account typically include $M_i^{(0)}$, $M_S^{(0)}$, $M_S^{(-)}$, and M_SD_S, where D_S denotes the substitutional donor atom. The equilibrium concentrations of these species are related by equations similar to Eqs. (12) and (13), so that the metal segregation coefficient can be calculated in cases where parameter values are known. The time dependence of the gettering is substantially more complex, since the conversion between M_i and M_S occurs through the reversible reactions of Eqs. (1) and (2), and this produces a coupling to the mobile populations of vacancy and self-interstitial defects. The problem is nevertheless tractable through straightforward extensions of the formulations and numerical methods of solution previously applied to the time-dependent gettering of Fe in B-doped Si and the diffusion and trapping of Au in intrinsic Si.[15,37]

In summary, Si layers with a high level of p-type or n-type doping give rise to segregation gettering as a result of the combined effects of metal-dopant pairing and the energy reduction of charged species arising from the Fermi-level shift. The segregation coefficients can be large at lower temperatures but decrease rapidly with temperature, so that it is typical for the most beneficial gettering to occur below 700 or 800°C. The nature of the underlying physical processes is believed to be largely understood, but quantitative information allowing fully predictive modeling is available for only a few cases, most notably Fe in B-doped Si. Observations to date have tended to show stronger gettering in P-doped, n-type Si than in B-doped, p-type material for similar doping levels.

E. Phosphorus-diffusion gettering and nonequilibrium processes

When P diffuses into a Si wafer from a source such as $POCl_3$ gas at temperatures above about 850°C, a strong gettering effect concurrent with the P diffusion is observed. This method of gettering has received considerable attention in connection with polycrystalline solar-cell material because it is effective at temperatures sufficiently elevated to allow diffusion from the

entire, macroscopic active region of the device and because it provides binding strong enough to prevent or reverse metal-silicide precipitation at grain boundaries and other defects. (See, *e.g.*, Refs. 135-137.) The observed phenomenology has several aspects that have not been explained in terms of the equilibrium pairing and Fermi-level effects discussed in the preceding subsection. One such feature is simply the large magnitude of the metal enrichment in the gettering layer at elevated temperatures. For example, when a sample initially containing a uniform Co concentration of 4×10^{14} atoms/cm^3 was subjected to P in-diffusion at 920°C, the near-surface concentration rose to 3×10^{18} atoms/cm^3 while that in the nearby bulk dropped to 1.2×10^{13} atoms/cm^3.[138] Since the latter value is smaller than the solubility by an order of magnitude, it can be inferred that a process other than equilibrium metal-silicide precipitation is responsible, and one capable of producing a concentration difference greater than 5 orders of magnitude. In comparison, the enrichment factor attributable to equilibrium segregation under these conditions has been estimated to be ~100.[9] Similarly, Au concentration ratios of at least 10^6 with a final bulk concentration $<5\times10^{11}$ Au/cm^3 were reported following in-diffusion from a P source at 988°C, [20] whereas a concentration ratio of ~10^4 was estimated for equilibrium segregation alone.[139] Another noteworthy feature of the above Co results is that the concentration of gettered metal atoms drops immediately and rapidly with distance from the surface even when there is a plateau in P concentration, whereas equilibrium segregation should produce a corresponding plateau in the metal concentration profile.[138] Finally, studies of Co gettering that used $POCl_3/O_2/N_2$ gas of varying composition for the P source revealed an abrupt upward step in gettering within the Si matrix as a function of the growth rate of P silicate glass on the surface.[140] Observations such as these have led to the inference that, when gettering is concurrent with P in-diffusion at high concentrations, nonequilibrium, dynamical gettering processes involving self-interstitial defects operate in addition to the equilibrium effects considered in Section III.D. While full mechanistic understanding has still to be achieved, research has yielded significant insights, as discussed below.

A range of experimental evidence indicates that diffusion of P into Si at high concentrations causes the concentration of self-interstitial defects to increase by orders of magnitude from thermal equilibrium.[6,141] Theoretical analysis of the diffusion and interactions of the P and self-interstitials (I) at several levels of completeness and generality has shown that such supersaturation arises naturally from the existence of bound mobile P-I pairs.[142-144] In these calculations, the concentration of unpaired self-interstitials is constrained to its equilibrium value at the surface, which is expected to act as a sink; the interstitial concentration then rises with increasing depth as a result of the dissociation of the inwardly diffusing P-I complexes. Typical depth profiles from such modeling are reproduced in Fig. 13.[143] These particular results represent a fit to an experimentally measured P profile that was obtained when an initially abrupt distribution, produced by P ion implantation and fast laser annealing, was diffusion-broadened by annealing at 850°C for 30 minutes. The two-component shape of the P tail differs qualitatively from what would be expected for simple diffusion, and this is among the

characteristic manifestations of the self-interstitial supersaturation. Figure 13 also shows the predicted enhancement of the concentration [I] of unpaired self-interstitials relative to its equilibrium value $[I]_{eq}$. The fact that [I] is close to equilibrium in the near-surface region but orders of magnitude higher in the underlying bulk is centrally important to P-diffusion gettering, as will now be discussed.

A nonequilibrium concentration of self-interstitials is believed to influence metal gettering because of the reversible kick-out reaction of Eq. (1), whereby an interstitial Si atom exothermically replaces a substitutional metal atom leaving a metal interstitial, thereby altering the populations of the metal states. In the presence of multiple charge states the reaction can be written more generally as

$$M_i^{(\sigma)} \leftrightarrow M_S^{(\sigma')} + I^{(\sigma'')} + (\sigma'+\sigma''-\sigma)e^- \tag{16}$$

where σ is the integer charge state. If local equilibrium between the reacting species is maintained everywhere in the specimen at all times, a condition believed to be well satisfied at the elevated temperatures of interest, application of detailed balance to the reaction of Eq. (16) gives[21]

$$\frac{\left[M_i^{(\sigma)}\right]}{\left[M_S^{(\sigma')}\right]\left[I^{(\sigma'')}\right]} = \frac{\left[M_i^{(\sigma)}\right]^{sol}}{\left[M_S^{(\sigma')}\right]^{sol}\left[I^{(\sigma'')}\right]_{eq}} \tag{17}$$

where $\left[M_i^{(\sigma)}\right]^{sol}$ and $\left[M_S^{(\sigma')}\right]^{sol}$ represent solubilities in equilibrium with the metal-silicide phase for a given Fermi energy as discussed in Section III.A, and $\left[I^{(\sigma')}\right]_{eq}$ is the self-interstitial concentration when the system is in complete thermodynamic equilibrium. Here it has been assumed that the metal and self-interstitial concentrations are small in comparison to the majority carrier concentration so that the Fermi level is not affected by the metal atoms. Equation (17) directly exhibits the way in which the influence of self-interstitial supersaturation is superimposed on the equilibrium Fermi-level effects discussed in Section III.D; the ratio of interstitial metal atoms to substitutional metal atoms is seen to vary in proportion to the self-interstitial concentration.

It has been shown that the array of equations given by Eq. (17) can be combined into a single equation where the concentrations of the charged states of substitutional metal atoms and

of self-interstitials are summed.[21] Furthermore, concentration interrelationships due to pairing reactions of the type

$$M_S^{(\sigma)} + P^{(\sigma')} \leftrightarrow M_S P^{(\sigma'')} + (\sigma''+\sigma'-\sigma)e^- \tag{18}$$

can be incorporated into the same equation when it is noted that the P concentrations of interest are either zero or large compared to the metal concentration. The result is[21]

$$\frac{\left[M_i^{(\sigma)}\right]}{([M_S]+[M_S P])[I]} = \frac{\left[M_i^{(\sigma)}\right]^{sol}}{\left([M_S]^{sol}+[M_S P]^{sol}\right)[I]_{eq}} \tag{19}$$

where the absence of a charge-state designation implies a sum over charge states. The equation is also valid when $M_i^{(\sigma)}$ is replaced by M_i. The increase of $[M_i]$ with [I] discussed above is again apparent.

The time-dependent depth profile of the total metal concentration [M] during P-diffusion gettering can be calculated by evaluating the atomic flux due to migration of the mobile interstitial component M_i. As already noted, most of the metal impurities are in the neutral charge state when occupying the interstitial site in intrinsic or n-type Si; the notable exception is Cu, whose charge is +1. Hence, the total atomic flux is given by Eq. (15). This equation can be reformulated in terms of [M] by using Eq. (19) in conjunction with equations for the equilibrium quantities that appear on the right-hand side. The required values of [P] and [I] can be obtained from a treatment of the P in-diffusion; this problem becomes separable upon making the usually valid assumption that [M] is sufficiently small to have negligible influence on [P] and [I]. Such calculations will be illustrated and compared with experiment in Section IV for the case of Au. Among the resulting insights is that the rate as well as the magnitude of P-diffusion gettering is substantially enhanced by the supersaturation of self-interstitials in the bulk, since this supersaturation causes a larger fraction of the metal atoms to be in mobile interstitial solution.

It is instructive to treat the above problem in quasi-steady-state and thereby derive an approximate equation for the metal concentration in the gettering region relative to that in the underlying bulk. This is accomplishing by setting $\bar{J}_M = 0$ in Eq. (15), which with manipulation yields the concentration ratio

$$G_{pdg} \equiv \frac{[M]^{(surf)}}{[M]^{(bulk)}} = \left(\frac{\left(\frac{[I]^{(bulk)}}{[I]_{eq}}\right)\left(\frac{[M]_{sol}}{[M_i]_{sol}}\right)}{\left(\frac{[I]^{(bulk)}}{[I]_{eq}}\right)+\left(\frac{[M]_{sol}}{[M_i]_{sol}}\right)-1} \right) K_{dop} \tag{20}$$

where K_{dop} is the equilibrium segregation coefficient arising solely from the Fermi-level shift and atomic pairing with the P dopant as discussed in Section III.D, and $[I]_{eq}$ and the metal solubilities are for intrinsic Si.[21] The expression within brackets on the right gives the enhancement of the gettering effect that arises from the supersaturation of self-interstitials at depths beyond the gettering layer. This effect has been termed "injection gettering."

Equation (20) allows one to distinguish several regimes of injection gettering. First, it is apparent that the effect of the self-interstitial supersaturation in the bulk is important primarily for metals such as Au, Pt, and Zn that have a substantial component in solution in intrinsic Si, so that $[M]_{sol} >> [M_i]_{sol}$; when the metal in solution is instead mostly interstitial, as for Pd and the 3d element from Ti to Cu, the enhancement factor remains close to 1, and $G_{pdg} \approx K_{dop}$. Furthermore, in the case of the substitutional solutes, $G_{pdg} \approx ([I]^{(bulk)} / [I]_{eq}) K_{dop}$ for self-interstitial supersaturations such that $([I]^{(bulk)} / [I]_{eq}) << ([M]_{sol} / [M_i]_{sol})$, whereas for $([I]^{(bulk)} / [I]_{eq}) >> ([M]_{sol} / [M_i]_{sol})$ one has the limiting condition $G_{pdg} \approx ([M]_{sol} / [M_i]_{sol}) K_{dop}$. The large magnitude of the injection effect is exemplified by applying Eq. (20) to the representative case of Au gettering at 900°C, where it has been estimated that $([M]_{sol} / [M_i]_{sol}) \sim 10^2$,[145] and $([I]^{(bulk)} / [I]_{eq})$ is expected to be $\sim 10^2$–10^3 depending upon the conditions of P in-diffusion. This calculation yields the estimate $(G_{pdp} / K_{dop}) \sim 10^2$, which is consistent with experimental observations.[20]

The considerations reviewed to this point do not provide a complete description of P-diffusion gettering because they fail to include several additional effects that are observed experimentally or expected on theoretical grounds. Among these effects is that, as already discussed, a nonequilibrium enhancement of P-diffusion gettering appears to take place for 3d elements such as Co that are primarily interstitial in intrinsic Si. This is not predicted by Eq. (20) since, as noted above, equating $[M]_{sol}$ to $[M_i]_{sol}$ gives $G_{pdg} = K_{dop}$. The mechanism underlying the strong gettering observed in such cases remains to be fully understood, although tentative ideas have been propounded as discussed below.

Another new feature emerges when the conditions of P injection are such as to increase the near-surface concentration of P beyond its solubility, giving rise to SiP precipitation in the near-surface region. An example of such precipitation is seen in the high-resolution cross-section TEM micrograph of Fig. 14a, obtained after exposure of Si to P_2O_5/N_2 gas at 900°C.[146] The SiP particle has grown inward from the interface between the Si and a P silicate glass (PSG) that formed on the surface. The growth of SiP is associated with a volume expansion, which is believed to be accommodated by the injection of about 1.5 Si interstitials per formula unit into the Si lattice. Epitaxial growth of Si occurs in the vicinity of the SiP particle, as seen from the displacement of the Si surface upward from its initial location indicated by the dashed white line, and this has been taken as evidence that at least some of the injected interstitials move to the surface sink. An influence of such SiP precipitation on gettering is indicated by metal-silicide

precipitation at the SiP particles when the wafer contains metal impurities. This is illustrated by the $NiSi_2$ precipitate imaged in Fig. 14b,[146] and a similar effect has been found during P-diffusion gettering of Pt.[75,147] It has been suggested that the self-interstitial flux in the vicinity of the SiP particles induces redistribution of the metal atoms and thereby causes a local supersaturation which gives rise to the observed metal-silicide precipitation,[9] in analogy to radiation-induced precipitation.[148] A mathematical formulation of these processes has not been reported for gettering, however.

Yet another effect not included in Eq. (20) is the probable influence of self-interstitial supersaturation on metal-silicide precipitation in the bulk region of the wafer. This arises from the volume change associated with the precipitation, which can be accommodated by the generation or annihilation of self-interstitials. In the case of Cu_3Si, for example, where the volume change is positive, precipitation should be inhibited, whereas the opposite effect should occur for $FeSi_2$, where the volume change is negative. This effect has still to be treated quantitatively or investigated experimentally.

In summary, P-diffusion gettering is an exceptionally effective method for removing metal impurities from Si at elevated temperatures, with concentration ratios as large as 10^6 reported for temperatures above 900°C. The attractiveness of the process is increased by the fact that it can be combined with junction formation in photovoltaic devices. A body of experimental and theoretical evidence supports the view that such gettering arises in part from the nonequilibrium injection of self-interstitial defects. Detailed mechanistic interpretation and the resultant mathematical modeling have yielded a semiquantitative-to-quantitative description for predominantly substitutional metals such as Au under conditions where metal-silicide precipitation does not occur. Understanding remains incomplete, however, for P-diffusion gettering of the predominantly interstitial 3d metals and for cases where the gettering is accompanied by metal-silicide precipitation.

IV. MODELING OF GETTERING AND IMPLICATIONS FOR DEVICE PROCESSING

The discussion of mechanisms in Section III included equations that enable modeling of the transport and reactions of the metal atoms under conditions relevant to device processing. Here, we describe such calculations for selected cases to exemplify important characteristics of the various approaches to gettering while also illustrating the mathematical procedures. We begin by considering metal-silicide precipitation, both at SiO_2 precipitates distributed through the bulk of the wafer (internal gettering), and at nucleation sites such as defects and cavities introduced into the near-surface region on the back side of the wafer (back-side gettering). In the second case study, B-Si precipitates are discussed as an example of a segregation-type gettering sink that can be introduced in proximity to the device region. The third part of the discussion

deals with gettering by electronic dopants; here the example is the reaction of Fe with B acceptors, with the B either ion-implanted into a layer beneath the device zone or present within a highly doped Si substrate beneath an epitaxial device layer. Finally, we present modeling of P-diffusion gettering.

Gettering through metal-silicide precipitation will be exemplified by the important and extensively investigated case of Fe. Since this solute is predominantly interstitial, the previously noted complications arising from occupation of substitutional sites can be neglected. (For a treatment of the more complicated situation where substitutional as well as interstitial solution sites are populated, see, *e.g.*, the analysis of Au gettering in Ref. 37.) In one dimension the governing equation is

$$\frac{\partial[M_i]}{\partial t} = D_i \frac{\partial^2[M_i]}{\partial x^2} - \frac{\partial[M_{sil}]Si}{\partial t} . \qquad (21)$$

Here the first term on the left-hand side takes account of diffusion, while the second term reflects the precipitation reaction and is evaluated using Eqs. (3) and (6). We consider first the situation where SiO_2 precipitates acting as $FeSi_2$ nucleation sites are distributed uniformly through the wafer except in a 10-μm depleted zone at the surface where the device is constructed. Such a precipitate distribution is routinely achieved through appropriate annealing of CZ Si. The effective radius of the sinks is taken to be 22 nm and the number per unit volume 2.5×10^{11} cm^{-3}, corresponding to a representative experimental observation.[13] The diffusion coefficient of the Fe is equated to $(9.5\times10^{-4}$ $cm^2/s)\exp(-0.65$ eV/kT),[38] the Fe solubility in equilibrium with its metal silicide is $\exp(8.2 - 2.94$ eV/kT),[5] and the thickness of the wafer is 0.5 mm. The simulation is carried out for isothermal annealing with an initial condition where the Fe is uniformly distributed in solution at a concentration of 1×10^{-12} atoms/cm^3. Equation (21) is solved numerically by dividing the x axis into finite elements and applying a stiff integrator as described elsewhere.[149]

Results from the above calculation are presented in Fig. 15, where the solution concentration at a depth of 1 μm within the 10-μm precipitate-free region is given as a function of time at three temperatures. The Fe undergoes diffusion-limited redistribution to the SiO_2 particles, where precipitation of $FeSi_2$ takes place until, ultimately, the solution concentration of Fe is equal to its solubility throughout the wafer. Rather low gettering temperatures are necessary to reduce the concentration into the desirable range below 10^{10} atoms/cm^3, although the diffusion rate is still sufficient to accomplish the reduction in experimentally convenient times. One important implication, however, is that the gettering anneal should not be followed by high-temperature processing, which will reintroduce the metal into solution. A further consideration is that, since such gettering reduces the Fe concentration to the solubility and no

further, it may not be effective in suppressing unwanted metal-silicide formation at such critical device sites as gate oxides.

Analogous calculations were carried out for the case where the sites for metal-silicide precipitation are localized on the back side of the wafer, and the results are shown as dashed lines in Fig. 15. While the asymptotic solution concentration is unchanged from internal gettering, the time to reach it is increased roughly as the square of the diffusion distance, or about three orders of magnitude. This makes the lower-concentration region in the figure inaccessible for most purposes. Moreover, such large diffusion times and distances increase considerably the extent to which metal impurities can precipitate at defects or interfaces within the device region instead of at the intended sinks, and this unwanted distribution tends to persist because the metal chemical potential is to first order identical at all precipitation sites. This consideration reinforces the desirability of having the gettering centers proximate to the device region. A related implication is that gettering by metal-silicide precipitation has limited applicability to devices that occupy macroscopic thicknesses of Si, such as solar cells. In these cases the diffusion distance to the gettering sinks is necessarily large, and the resultantly high probability of metal atoms being intercepted by defects is unavoidable. One solution is to employ gettering mechanisms that provide metal chemical potentials below those of the corresponding metal-silicide phases and that as a consequence induce dissolution of such phases. This property is shared by the processes to be considered in the remainder of the section.

The characteristics of gettering by a segregation-type mechanism will be illustrated by modeling the binding of Fe within a buried layer containing precipitates of the B-Si phase discussed in Section III.B. The layer is taken to be located beneath the device region at a depth of 10 μm and to contain a B areal density of 1×10^{17} atoms/cm^2 within the B-Si phase. At zero time, the Fe is in solution at a concentration of 1×10^{12} atoms/cm^3 throughout the 0.5-mm thickness of the wafer. For this calculation the final, reaction term in Eq. (21) is replaced by $\partial[M_{sp}]_{Si}/\partial t$, which is evaluated using Eqs. (7) and (8) and the results in Fig. 9. In Fig. 16 the calculated solution concentration at a depth of 1μm is plotted as a function of time for isothermal annealing at temperatures from 600 to 1000°C.

In its early stages, the behavior shown in Fig. 16 resembles that for metal-silicide precipitation in Fig. 15, with the gettering rate again being controlled by Fe diffusion to the sinks at 10 μm. Ultimately, however, the solution concentration in the presence of the B-Si phase reaches levels below the solid solubility, reflecting the strong segregation gettering. As a result, such gettering can induce the dissolution of metal-silicide precipitates, thereby providing the range of benefits discussed above. Another noteworthy difference is that the predicted solution concentration at 1 μm goes through a minimum with time rather than monotonically decreasing. This effect arises from the proportionality of the Fe solution concentration in the vicinity of the B-Si precipitates to the amount of Fe contained within these precipitates, as given by Eq. (7). At

times beyond that required for the diffusion to produce near equality of the solution concentrations at 1 μm and 10 μm, the continuing accumulation of Fe from the bulk of the wafer into the sinks causes the solution concentration in the entire near-surface region to rise until the Fe concentration is uniform throughout the wafer. This effect is evident in the calculated depth profiles for annealing at 800°C that are shown in Fig. 17.

We turn now to gettering by electronic dopants, and take as an example the binding of Fe within a highly B-doped region of the Si wafer. Two cases are modeled: in one, the device region is a 10-μm epitaxial layer of intrinsic Si on a highly doped wafer of 0.5-mm thickness containing 1×10^{19} B/cm^3; in the other case, the B-containing region is a 0.5-μm layer with 1×10^{19} B/cm^3 located at a depth of 10 μm, similar to what might be formed by ion implantation. The initial condition is again a uniform solution concentration of 1×10^{12} Fe/cm^3. The governing one-dimensional equation is

$$N_{Si}\frac{\partial[M]}{\partial t} = -\frac{\partial J_M}{\partial x} \tag{22}$$

where [M] is the total metal atomic fraction $[M_i^{(0)}]+[M_i^{(+)}]+[M_iA_S]$, J_M is the atomic flux given by Eq. (15), and at any given depth the concentrations are interrelated by Eqs. (12) and (13). Parameters are evaluated as discussed in Section III.D, with $(E_F - E_V)$ being calculated as a function of depth under the approximation of net charge neutrality at each depth. The problem is again solved numerically by finite-element methods. Results are given in Fig. 18, where the solution concentration of Fe at 1 μm is plotted as a function of time.

The computational results in Fig. 18 illustrate the point that gettering by electrical dopants is an effective segregation-type mechanism, but one that operates at lower temperatures than some of the other processes considered herein. An important additional motivation for the use of this method is the beneficial electrical isolation of devices that arises from the underlying p^+ layer. The doped substrate is seen in the figure to produces a larger gettering effect than the microscopic doped layer as a result of the greater gettering volume. In the presence of the thin gettering layer there is a minimum in the near-surface concentration as a function of time, as was also found for the segregation gettering to a layer of B-Si precipitates; the cause is again the accumulation of metal atoms from the underlying bulk into the gettering region, giving rise there to an increase in metal chemical potential.

The final example of modeling concerns P-diffusion gettering of Au. We consider a case where the results of a detailed experimental study[20] were subsequently modeled on the basis of the equilibrium and nonequilibrium physical processes discussed in Sections III.D and III.E.[139] This complex problem entailed computation of the time-dependent concentration-versus-depth profiles of P and self-interstitial defects, which were then used to treat the combined influences of the Fermi-level shift, P-Au pairing, and self-interstitial gradients on the time-dependent depth

profile of metal atoms. Agreement with the measured concentration profiles of P was achieved through adjustment of some less accurately known parameters and the inclusion of mobile P-vacancy clusters in addition to the mobile P-I defects cited in Section III.E. The transport and reactions of the Au atoms were then model with no further adjustment of parameters.

Selected results from such modeling[139] are compared with experimental results[20] in Fig. 19. At the beginning of the experiment, the Si wafer contained a uniform Au concentration of ~3×10^{14} atoms/cm^3. Phosphorus-diffusion gettering was carried out by in-diffusing the P at 988°C for 30 minutes, followed by cooling at 5°C/minute to 900°C and then more rapidly to room temperature. The depth profiles of P and Au at this point, as measured by SIMS, are shown in Fig. 19(a) together with the computed results for [P_S], [I], [Au], [Au_S], and [Au_i]. The quantitative agreement between experiment and theory for [Au] occurred without adjustment of parameters and therefore reinforces the validity of the mechanistic interpretation. Assuming equilibrium segregation alone without the added influence of self-interstitial injection gives a near-surface enrichment of the Au concentration about two orders of magnitude smaller than observed, indicating the importance of the nonequilibrium effects. In this case the P-diffusion gettering has reduced the Au concentration in the bulk of the wafer by about three orders of magnitude. The specimen was lastly subjected to a further anneal at 1150°C for 15 minutes followed by rapid cooling, in this case with no P source at the surface, and [P] and [Au] were again measured by SIMS. This produced considerable additional evolution of the depth profiles, again in good agreement with predictions of the theoretical model.

V. CONCLUSION

The work of numerous researchers extending over several decades has yielded extensive information on the properties of transition metals in Si and on the binding reactions that can be used for gettering. As detailed in this article, at least five distinct types of gettering mechanism have been identified, and fundamental understanding has in a number of instances advanced to a semiquantitative or quantitative level allowing realistic predictive modeling. Nevertheless, a range of mechanistic issues remains to be resolved by further research. In the case of metal-silicide precipitation, the centrally important energetics and kinetics of nucleation and growth at defects are understood only qualitatively or semiquantitatively, and incompletely. The related issue of metal-atom trapping at lattice defects has hardly been explored except for the internal surfaces associated with cavities, where the binding reactions have been characterized only to first-order. The pairing of metals with electrical dopants has been studied in depth for a few cases, but such work has encompassed only a fraction of the combinations of interest. Among the stronger gettering effects known are those associated with metal segregation into second phases, specifically molten Al-Si and B silicides, yet the literature reports little exploration of other phases that might prove still more effective. Lastly, the understanding and exploitation of

dynamical processes to augment equilibrium gettering mechanisms has been largely limited to P-diffusion gettering, where the observed phenomenology has yet to be fully explained. Hence it is arguable that the volume of research remaining to be done in this field is not small in comparison to what has gone before. Moreover, the practical need for in-depth understanding is ever greater with the increasing complexity and impurity sensitivity of Si devices.

ACKNOWLEDGEMENTS

S. M. Myers was supported at Sandia National Laboratories by the U. S. Department of Energy under Contract DE-AC04-94AL85000. Sandia is a multiprogram laboratory operated by Sandia Corporation, a Lockheed Martin Company, for the U. S. Department of Energy. M. Seibt and W. Schröter were supported at the University of Göttingen by the Sonderforschungsbereich 345 and the BMBF.

REFERENCES

1. K. Graff, Metal Impurities in Silicon-Device Fabrication (Springer, Berlin, 1995).
2. International Technology Roadmap for Semiconductors: 1999 edition (Semiconductor Industry Assoc., Austin, TX, 1999), p. 109.
3. Crystalline Defects and Contamination: Their Impact and Control in Device Manufacturing, edited by B. O. Kolbesen, C. Claeys, P. Stallhofer, and F. Tardif (Electrochem. Soc., Pennington, NJ, Proc. Vol. 93-15,1993).
4. Crystalline Defects and Contamination: Their Impact and Control in Device Manufacturing II, edited by B. O. Kolbesen, P. Stallhofer, C. Claeys, and F. Tardif (Electrochem. Soc., Pennington, NJ, Proc. Vol. 97-22, 1997).
5. E. R. Weber, Appl. Phys. A **30**, 1 (1983).
6. U. M. Gösele and T. Y. Tan, in Materials Science and Technology, vol. 4: Electronic Structure and Properties of Semiconductors, edited by W. Schröter (VCH, New York, 1991) pp. 197-228.
7. W. Schröter and M. Seibt, in Properties of Crystalline Silicon, edited by R. Hull (INSPEC, London, 2000), pp.543-572, in press.
8. A. A. Istratov, C. Flink, H. Hieslmair, E. R. Weber, and T. Heiser, Phys. Rev. Lett. **81**, 1243 (1998).
9. W. Schröter, M. Seibt, and D. Gilles, in Materials Science and Technology, vol. 4: Electronic Structure and Properties of Semiconductors, edited by W. Schröter (VCH, New York, 1991) pp. 539-589.
10. J. Wong-Leung, D. J. Eaglesham, J. Sapjeta, D. C. Jacobson, J. M. Poate, and J. S. Williams, J. Appl. Phys. **83**, 580 (1998), and citations therein.
11. M. Seibt, H. Hedemann, A. A. Istratov, F. Riedel, A. Sattler, and W. Schröter, Phys. Stat. Sol. A **171**, 301 (1999), and citations therein.
12. D. Gilles, E. R. Weber, and S.-K. Hahn, Phys. Rev. Lett. **64**, 196 (1990).
13. H. Hieslmair, A. A. Istratov, S. A. McHugo, C. Flink, and E. R. Weber, J. Electrochem. Soc. **145**, 4259 (1998).
14. D. Gilles, W. Schröter, and W. Bergholz, Phys. Rev. B **41**, 5770 (1990).
15. P. A. Stolk, J. L. Benton, D. J. Eaglesham, D. C. Jacobson, J.-Y. Cheng, J. M. Poate, S. M. Myers, and T. E. Haynes, Appl. Phys. Lett. **68**, 51 (1996).
16. S. A. McHugo, R. J. McDonald, A. R. Smith, D. L. Hurley, and E. R. Weber, Appl. Phys. Lett. **73**, 1424 (1998).
17. R. D. Thompson and K. N. Tu, Appl. Phys. Lett. **41**, 440 (1982).
18. M. Apel, I. Hanke, R. Schindler, and W. Schröter, J. Appl. Phys. **76**, 4432 (1994).
19. H. Hieslmair, S. McHugo, and E. R. Weber, Conference Record of the Twenty Fifth IEEE Photovoltaic Specialists Conference - 1996 (IEEE, Piscataway, NJ, 1996) pp. 441-444.
20. E. Ö. Sveinbjörnsson and O. Engström, J. Appl. Phys. **73**, 7311 (1993).
21. E. Spiecker, M. Seibt, and W. Schröter, Phys. Rev. B **55**, 9577 (1997).

22. A. A. Istratov, H, Hieslmair, and E. R. Weber, Appl. Phys. A **69**, 13 (1999).
23. H. Tomita, M. Saito, and K. Yamabe, Mat. Sci. Forum **196-201**, 1991 (1995).
24. S. M. Myers, G. A. Petersen, D. M. Follstaedt, C. H. Seager, T. J. Headley, J. R. Michael, W. Deweerd, G. Koops, J. Verheyden, and H Pattyn, in Semiconductor Silicon 1998, edited by H. R. Huff, U. Gösele, and H. Tsuya (Electrochem. Soc., Pennington, NJ, Proc. Vol. 98-1, 1998), pp. 1150-1161.
25. R. A. Brown, O. Kononchuk, G. A. Rozgonyi, S. Koveshnikov, A. P. Knights, P. J. Simpson, and F. Gonzáles, J. Appl. Phys. **84**, 2459 (1998).
26. B. Shen, T. Sekiguchi, J. Jablonski, and K. Sumino, J. Appl. Phys. **76**, 4540 (1994).
27. B. Shen, X. Y. Zhang, K. Yang, P. Chen, R. Zhang, Y. Shi, Y. D. Zheng, T Sekiguchi, and K Sumino, Appl. Phys. Lett. **70**, 1876 (1997).
28. A. Ihlal, R. Rizk, O. B. M. Hardouin Duparc, J. Appl. Phys. **80**, 2665 (1996).
29. J. Wong-Leung, C. E. Ascheron, M. Petravic, R. G. Elliman, and J. S. Williams, Appl. Phys. Lett. **66**, 1231 (1995).
30. S. M. Myers, G. A. Petersen, and C. H. Seager, J. Appl. Phys. **80**, 3717 (1996).
31. T. Y. Tan, E. E. Gardner, and W. K. Tice, Appl. Phys. Lett. **30**, 175 (1977).
32. J. O. Borland, Semicond. Inter. 12, pp. 144-148, 154-157 (1989).
33. A. Borghesi, B. Pivac, A. Sassella, and A. Stella, J. Appl. Phys. **77**, 4169 (1995).
34. W. Frank, Def. and Diff. Forum **75**, 121 (1991).
35. D. Mathiot, Phys. Rev. B **45**, 13345 (1992).
36. H. Zimmermann and H. Ryssel, J. Electrochem. Soc. **139**, 256 (1992).
37. S. M. Myers and G. A. Petersen, Phys. Rev. B **57**, 7015 (1998).
38. T. Isobe, H. Nakashima, and K. Hashimoto, Jpn. J. Appl. Phys. **28**, 1282 (1989).
39. T. Heiser and A. Mesli, Appl. Phys. Lett. **58**, 2240 (1991).
40. H. Nakashima and K. Hashimoto, Mat. Sci. Forum **83-87**, 227 (1992).
41. L. Kalinowski and R. Seguin, Appl. Phys. Lett. 35, 211 (1979).
42. D. Mathiot and J. C. Pfister, J. Appl. Phys. **55**, 3518 (1984).
43. J. Utzig, J. Appl. Phys. **65**, 3868 (1989).
44. S. V. Koveshnikov and G. A. Rozgonyi, Appl. Phys. Lett. **66**, 860 (1995).
45. M. Seibt and W. Schröter, Phil. Mag. A **59**, 337 (1989).
46. F. H. Baumann and W. Schröter, Phys. Rev. B **43**, 6510 (1991).
47. S. P. Muraka, Silicides for VLSI Applications (Academic, New York, 1983), pp.99-131.
48. S. Hocine and D. Mathiot, Appl. Phys. Lett. **53**, 1269 (1988).
49. J.-W. Chen, A. G. Milnes, and A. Rohatgi, Solid State Electronics **22**, 801 (1979)
50. T. Sadoh and H. Nakashima, Appl. Phys. Lett. **58**, 1653 (1991).
51. D. Gilles, W. Bergholz, and W. Schröter, J. Appl. Phys. **59**, 3590 (1986).
52. H. Kitagawa and K. Hashimoto, Jpn. J. Appl. Phys. **16**, 857 (1977).
53. R. C. Dorward and J. S. Kirkaldy, Trans. AIME **242**, 2055 (1968).
54. D. Grünebaum, Th. Czekalla, N. A. Stolwijk, H. Mehrer, I. Yonenaga, and K. Sumino, Appl. Phys. A **53**, 65 (1991).

55. K. P. Lisiak and A. G. Milnes, Solid-State Electronics **18**, 533 (1975).
56. M. Jacob, P. Pichler, H. Ryssel, and R. Falster, J. Appl. Phys. **82**, 182 (1997).
57. J. Hauber, W. Frank, and N. A. Stolwijk, Mat. Sci. Forum **38-41**, 707 (1989).
58. F. S. Ham, J. Phys. Chem. Solids **6**, 335 (1958).
59. P. M. Richards, J. Chem. Phys. **85**, 3520 (1986).
60. P. M. Richards, Phys. Rev. B **35**, 248 (1987).
61. M. Seibt, in Semiconductor Silicon 1990, edited by H. R. Huff, K. G. Barraclough, and J. Chikawa (Electrochem Soc., Pennington, NJ, 1990), pp.663-674.
62. M. Seibt, M. Griess, A. A. Istratov, H. Hedemann, A. Sattler, and W. Schröter, Phys. Stat. Sol. A **166**, 171 (1998).
63. A. A. Istratov, C. Flink, H. Hieslmair, S. A. McHugo, and E. R. Weber, Mat. Sci. Eng. B, in press.
64. A. A. Istratov, H. Hedemann, M. Seibt, O. F. Vyvenko, W. Schröter, T. Heiser, C. Flink, H. Hieslmair, and E. R. Weber, J. Electrochem. Soc. **145**, 3889 (1998).
65. H. Hedemann and W. Schröter, J. Phys. III France **7**, 1389 (1997).
66. W. Schröter, J. Kronewitz, U. Gnauert, F. Riedel, and M. Seibt, Phys. Rev. B **52**, 13726 (1995).
67. J. Wong-Leung, J. S. Williams, and E. Nygren, Nucl. Instrum. Meth. Phys. Res. B **106**, 424 (1995).
68. M. Seibt and K. Graff, J. Appl. Phys. 63, 4444 (1988); and Mat. Res. Soc. Symp. Proc. **104**, 215 (1988).
69. H. Takahashi, H. Yamada-Kaneta, and M. Suezawa, Jpn. J. Appl. Phys. **37**, 1689 (1998).
70. H. Hieslmair, A. A. Istratov, T. Heiser, and E. R. Weber, J. Appl. Phys. **84**, 713 (1998).
71. H. J. Geipel and W. K. Tice, Appl. Phys. Lett. **30**, 325 (1977).
72. R. Falster, Z. Laczik, G. R. Booker, A. R. Bhatti, and T. Török, Mat. Res. Soc. Symp. Proc. **262**, 945 (1992).
73. B. Shen, T. Sekiguchi, J. Jablonski, and K. Sumino, J. Appl. Phys. **76**, 4540 (1994).
74. B. Shen, X. Y. Zhang, K. Yang, P. Chen, R. Zhang, Y. Shi, Y. D. Zheng, T. Sekiguchi, and K Sumino, Appl. Phys. Lett. **70**, 1876 (1997).
75. M. Seibt, M. Apel, A. Döller, H. Ewe, E. Spiecker, W. Schröter, and A. Zozime, in Semiconductor Silicon 1998, edited by H. R. Huff, U. Gösele, and H. Tsuya (Electrochem. Soc., Pennington, NJ, Proc. Vol. 98-1, 1998), pp. 1064-1079.
76. T. M. Buck, K. A. Pickar, J. M. Poate, and C.-M. Hsieh, Appl. Phys. Lett. **21**, 485 (1972).
77. T. E. Seidel, R. L. Meek, and A. G. Cullis, J. Appl. Phys. **46**, 600 (1975).
78. T. Kuroi, Y. Kawasaki, S. Komori, K. Fukumoto, M. Inuishi, K. Tsukamoto, H. Shinyashiki, and T. Shingyoji, Jpn. J. Appl. Phys. **32**, 303 (1993).
79. V. Raineri, P. G. Fallica, G. Percolla, A. Battaglia, M. Barbagallo, and S. U. Campisano, J. Appl. Phys. **78**, 3727 (1995).
80. W. Skorupa and R. A. Yankov, Mat. Chem. Phys. **44**, 101 (1996).

81. W. Deweerd, T. Barancira, S. Bukshpan, S. Demuynck, G. Langouche, K. Milants, R. Moons, J. Verheyden, and H. Pattyn, Phys. Rev. B **53**, 16637 (1996)
82. S. V. Koveshnikov and G. A. Rozgonyi, J. Appl. Phys. **84**, 3078 (1998).
83. M. Tamura, Mat. Sci. Reps. **6**, 141 (1991).
84. E. Chason, S. T. Picraux, J. M. Poate, J. O. Borland, M. I. Current, T. Diaz de la Rubia, D. J. Eaglesham, O. W. Holland, M. E. Law, C. W. Magee, J. W. Mayer, J. Melngailis, and A. F. Tasch, J. Appl. Phys. **81**, 6513 (1997).
85. R. Hull, A. E. White, K. T. Short, and J. M. Bonar, J. Appl. Phys. **68**, 1629 (1990).
86. X. W. Lin, J. Desimoni, H. Bernas, Z. Liliental-Weber, and J. Washburn, Mat. Res. Soc. Symp. Proc. **320**, 97 (1994).
87. J. Wong-Leung, J. S. Williams, R. G. Elliman, E. Nygren, D. J. Eaglesham, D. C. Jacobson, and J. M Poate, Nucl. Instrum. Methods B **96**, 253 (1995).
88. D. M. Follstaedt, S. M. Myers, G. A. Petersen, and J. W. Medernach, J. Electronic Mat. **25**, 151 (1996).
89. J. Wong-Leung, J. S. Williams, A. Kinomura, Y. Nakano, Y. Hayashi, and D. J. Eaglesham. Phys. Rev. B **59**, 7990 (1999).
90. R. Sundaresan, D. E. Burk, and J. G. Fossum, J. Appl. Phys. **55**, 1162 (1984).
91. L. A. Verhoef, P.-P. Michiels, S. Roorda, W. C. Sinke, and R. J. C. Van Zolingen, Mat. Sci. Eng. B **7**, 49 (1990).
92. P. Sana, A. Rohatgi, J. P. Kalejs, and R. O. Bell, Appl. Phys. Lett. **64**, 97 (1994).
93. S. Martinuzzi, O. Porre, I. Périchaud, and M. Pasquinelli, J. Phys. III (France) **5**, 1337 (1995).
94. S. M. Joshi; U. M. Gösele, and T. Y. Tan, J. Appl. Phys. **77**, 3858 (1995).
95. S. M. Myers, G. A. Petersen, T. J. Headley, J. R. Michael, T. L. Aselage, and C. H. Seager, Nucl. Instrum. Methods B **127-128**, 291 (1997).
96. T. J. Headley, J. R. Michael, S. M. Myers, G. A. Petersen, T. L. Aselage, and J. Bruley, in Microscopy and Microanalysis '97 (Microscopy Soc. of Amer., 1997), pp. 455-456.
97. W. Deweerd, G. Koops, H. Pattyn, S. M. Myers, T. L. Aselage, T. J. Headley, and G. A. Petersen, Europhys. Lett. **44**, 707 (1998).
98. Binary Alloy Phase Diagrams, edited by T. B. Massalski, J. L. Murray, L. H. Bennett, and H. Baker (ASM, Metals Park, Ohio, 1986).
99. M. E. Schlesinger, Chem. Rev. **90**, 607 (1990).
100. T. Y. Tan, R. Gafiteanu, S. M. Joshi, and U. Gösele, in Semiconductor Silicon 1998, edited by H. R. Huff, U. Gösele, and H. Tsuya (Electrochem. Soc., Pennington, NJ, Proc. Vol. 98-1, 1998), pp. 1050-1063.
101. S. Frabboni, G. Lulli, P. G. Merli, A. Migliori, and R. Bauer, Ultramicroscopy **35**, 265 (1991).
102. A. Armigliato, D. Nobili, P. Ostoja, M. Servidori, and S. Solmi, in Semiconductor Silicon, edited by H. R. Huff and E. Sirtl (Electrom. Soc., Pennington, NJ, 1977) pp. 638-647.
103. T. L. Aselage, J. Mat. Res. **13**, 1786 (1988).

104. S. M. Myers, D. M. Follstaedt, and D. M. Bishop, Mat. Res. Soc. Symp. Proc. **316**, 33 (1994).
105. B. Mohadjeri, J. S. Williams, and J. Wong-Leung, Appl. Phys. Lett. **66**, 1889 (1995).
106. M. H. F. Overwijk, J. Politiek, R. C. M. de Kruif, and P. C. Zalm, Nucl. Instrum. Methods Phys. Res. B **96**, 257 (1995).
107. A. Cacciato, C. M. Camalleri, G. Franco, V. Raineri, and S. Coffa, J. Appl. Phys. **80**, 4322 (1996).
108. S. A. McHugo, E. R. Weber, S. M. Myers, and G. A. Petersen, Appl. Phys. Lett. **69**, 3060 (1996).
109. K. C. Hall, R. D. Goldberg, T. D. Lowes, P.J. Simpson, I. V. Mitchell, and G. C. Weatherly, Can. J. Phys. **74**, S248 (1996).
110. S. M. Myers and D. M. Follstaedt, J. Appl. Phys. **79**, 1337 (1996).
111. A. Kinomura, J. S. Williams, J. Wong-Leung, and M. Petravic, Nucl. Instrum. Methods Phys. Res. B **127-128**, 297 (1997).
112. J. Min, P. K. Chu, X. Lu, S. S. K. Iyer, and N. W. Cheung, Thin Solid Films **300**, 64 (1997).
113. S. A. McHugo, E. R. Weber, S. M. Myers, and G. A. Petersen, J. Electrochem. Soc. **145**, 1400 (1998).
114. F. Schiettekatte, C. Wintgens, and S. Roorda, Appl. Phys. Lett. **74**, 1857 (1999).
115. M. Zhang, C. Lin, X. Duo, Z. Lin, and Z. Zhou, J. Appl. Phys. **85**, 94 (1999)
116. R. Plass and L. D. Marks, Sur. Sci. **380**, 497 (1997).
117. W. R. Wampler, Mat. Res. Soc. Symp. Proc. **440**, 493 (1997).
118. D. M. Follstaedt, Appl. Phys. Lett. **62**, 1116 (1993).
119. D. J. Eaglesham. A. E. White, L. C. Feldman, N. Moriya, and D. C. Jacobson, Phys. Rev. Lett. **70**, 1643 (1993).
120. R. Kögler, J. R. Kaschny, R. A. Yankov, P. Werner, A. B. Danilin, and W. Skorupa, Solid State Phenom. **57-58**, 63 (1997).
121. A. M. Mazzone, Phys. Stat. Sol. A **95**, 149 (1986).
122. R. Kögler, A. Peeva, W. Anwand, P. Werner, A. B. Danilin, and W. Skorupa, Solid State Phenom. **69-70**, 235 (1999).
123. H. Lemke, Phys. Stat. Sol. A **64**, 215 (1981).
124. L. C. Kimerling and J. L. Benton, Physica B **116**, 297 (1983).
125. S. M. Sze, Physics of Semiconductor Devices (John Wiley, New York, 1981) pp.74-84.
126. C. H. Seager, S. M. Myers, R. A. Anderson, W. L. Warren, and D. M. Follstaedt, Phys. Rev. B **50**, 2458 (1994).
127. F. G. Kirscht, M. B. Shabani, T. Yoshimi, S.-B Kim, B. Snegirev, C. Wang, L. Williamson, K. Takashima, P. Taylor, and D. Lange, Solid State. Phenom. **57-58**, 355 (1997).
128. G. Obermeier and D. Huber, J. Appl. Phys. **81**, 7345 (1997).

129. M. Miyazaki, S. Miyazaki, S. Ogushi, T. Ochiai, M. Sano, and T. Skhigematsu, Jpn. J. Appl. Phys. **36**, L380 (1997).
130. J. L. Benton, P. A. Stolk, D. J. Eaglesham, D. C. Jacobson, J.-Y. Cheng, J. M. Poate, N. T. Ha, T. E. Haynes, and S. M. Myers, J. Appl. Phys. **80**, 3275 (1996).
131. H. Lemke, Phys. Stat. Sol. A **76**, 223 (1983).
132. T. Heiser, A. A. Istratov, C. Flink, and E. R. Weber, Mat. Sci. Eng. B **58**, 149 (1999).
133. A. Chantre and D. Bois, Phys. Rev. B **31**, 7979 (1985).
134. T. A. O'Shaughnessy, H. D. Barber, D. A. Thompson, and E. L. Heasell, J. Electrochem. Soc. **121**, 1350 (1974).
135. I. Perichaud and S. Martinuzzi, J. Phys. III (France) **2**, 313 (1992).
136. M. Loghmarti, K. Mahfoud, J. Kopp, J. C. Muller, and D. Sayah, Phys. Stat. Sol. A **151**, 379 (1995).
137. S. Harashimha and K. A. Rohatgi, IEEE Trans. Electron. Dev. **45**, 1776 (1998).
138. R. Kühnapfel, W. Schröter, and D. Gilles, Mat. Sci. Forum **10-12**, 151 (1986); R. Kühnapfel, thesis, Göttingen University, 1987.
139. V. Kveder, W. Schröter, A. Sattler, and M. Seibt, Mater. Sci. and Eng. B 56 (1999), in press.
140. R. Kühnapfel and W. Schröter, in Semiconductor Silicon 1990, edited by H. R. Huff, K. G. Barraclough, and J.-I. Chikawa (Electrochem. Soc., Pennington, NJ, Proc. Vol. 90-7, 1990) pp. 651-662.
141. S. M. Hu, Mat. Sci. Eng. R **13**, 105 (1994).
142. F. F. Morehead and R. F. Lever, Appl. Phys. Lett. **48**, 151 (1986).
143. B. J. Mulvaney and W. B. Richardson, Appl. Phys. Lett. **51**, 1439 (1987).
144. M. Orlowski, Appl. Phys. Lett. **53**, 1323 (1988).
145. C. Boit, F. Lau, and R. Sittig, Appl. Phys. A **50**, 197 (1990).
146 A. Ourmazd and W. Schröter, Appl. Phys. Lett. **45**, 781 (1984).
147. A. Correia, B. Pichaud, A. Lhorte, and J. B. Quiorin, J. Appl. Phys. **79**, 2145 (1996).
148. G. Martin, Phil. Mag. A **38**, 131 (1978), and citations therein.
149. S. M. Myers, D. E. Amos, and D. K. Brice, J. Appl. Phys. **47**, 1812 (1976).

TABLE I. Solubility parameters for transition-metal solutes in intrinsic Si. The solubilities are obtained by substitution into Eqs. (3)-(5).

Metal	Eutectic (°C)	Soln. site	ΔH_{sil} (eV)	$\frac{\Delta S^o_{sil}}{k}$	$\Delta H_{liq}-\Delta H^{fus}_M$ (eV)	$\frac{\Delta S^o_{liq}-\Delta S^{fus}_M}{k}$	Range (°C)	Reference
Ti	1330	Interstitial	3.0	3.9			1000-1200	49,7
			3.05	4.2			950-1200	48
V	1400	Interstitial	4.04	11.0			950-1200	50
Cr	1335	Interstitial	2.79	4.7			900-1200	7
Mn	1142	Interstitial	2.81	7.3			900-1142	5
			2.78	6.9			920-1078	51
Fe	1206	Interstitial	2.94	8.2			900-1206	5
Co	1259	Interstitial	2.99	7.5			1000-1250	52,7
			2.83	7.6			700-1200	5
Ni	993	Interstitial	1.68	3.2			500-993	5
					1.25	-0.17		5,7
Cu	802	Interstitial	1.75	4.9			650-802	53
			1.49	2.4			500-802	5
					1.60	3.4		53
Pd	892	Interstitial	1.64	1.2			600-892	34,7
					1.34	-0.8		34,7

Metal	Eutectic (°C)	Soln. site	$\Delta H_{sil}-\Delta H_{sub}$	$\frac{\Delta S^o_{sil}-\Delta S^o_{sub}}{k}$	$\Delta H_{liq}-\Delta H^{fus}_M-\Delta H_{sub}$	$\frac{\Delta S^o_{liq}-\Delta S^{fus}_M-\Delta S^o_{sub}}{k}$		
Zn	419	Substitutional			2.61	8.2		54,7
Pt	979	Substitutional	2.43	7.0			800-950	55,7
			2.212	4.5			700-950	36
			3.45	16.4			680-842	56
					1.46	-0.1		57,7
					1.60	0.82		55,7
Au	363	Substitutional			1.92	2.8		7

FIGURE CAPTIONS

Figure 1. Diffusion coefficients of representative interstitial transition metals in Si, with charge state indicated where definitively known.[8,38-40] Included for comparison are the much smaller diffusion rates of two substitutional species, B and Si self-atoms. The horizontal dashed lines indicate approximate diffusivity thresholds for local atomic processes, proximity gettering, and back-side gettering.

Figure 2. High-resolution TEM image of $NiSi_2$ platelet lying on $Si(1\bar{1}1)$ lattice planes after rapid quenching of a Si(Ni) solution from 1050°C.[45] The associated rigid shift of the Si lattice is indicated by the white line.

Figure 3. Ostwald ripening of $NiSi_2$ precipitates during annealing at various temperatures after quenching of a Si(Ni) solution from 1050°C.[45] The anneal time is 20 minutes.

Figure 4. Solubilities of representative interstitial transition metals in Si below the eutectic temperature.[5,48] The solid lines show the range of experimental data, while the dashed lines are extrapolated.

Figure 5. Colony of Cu_3Si precipitates in Si after cooling of a Si(Cu) solution from 900°C.[62] (a) Low-magnification TEM micrograph showing planar arrangements of dislocation loops and Cu_3Si precipitates. (b) Detail showing Moiré contrast at silicide particles.

Figure 6. Reduction of Fe solution concentration due to $FeSi_2$ precipitation at SiO_2 particles at 280°C.[12] The initial Fe concentration is 7.2×10^{14} atoms/cm^3. The exponential decay is consistent with the diffusion-controlled kinetics represented by Eq. (6).

Figure 7. Effective density of SiO_2 sinks during $FeSi_2$ precipitation from solution for two SiO_2 densities and a range of temperatures, as derived by fitting of Eq. (6) to the experimentally measured decay of the Fe solution concentration.[13] The horizontal lines give the actual particle densities obtained from microscopy.

Figure 8. Phase-contrast TEM image of B-Si precipitate formed in Si by B ion implantation and subsequent annealing at 1100°C for 2 hours.[96] The pronounced, orientation-independent granularity of the particle image combined with the absence of an associated diffraction pattern are indicative of structural disorder.

Figure 9. Segregation coefficient for gettering of Fe by B-Si precipitates.[24] The precipitates were formed by B ion implantation and annealing and then equilibrated with Fe in solution at a concentration equal to its solid solubility.

Figure 10. Redistribution of Cu from a layer containing Cu_3Si to a cavity layer on the opposite side of the Si wafer.[110] The line shows a fitted model calculation based on diffusion-limited flow to a strong, saturable sink. The high-resolution TEM image of a cavity after gettering shows no evidence of metal-silicide precipitation, consistent with gettering by a chemisorption trapping mechanism.

Figure 11. Binding free energies of transition metals at cavity walls obtained from application of Eqs. (9)-(11) to gettering experiments.[30,37,110]

Figure 12. Predicted segregation coefficients for gettering of Fe in B-doped Si as a function of temperature and B concentration, obtained using Eqs. (12) and (13). The dashed curves show the effect of the dopant-induced Fermi-level shift alone, neglecting Fe-B pairing.

Figure 13. Theoretically calculated depth profiles associated with P diffusion at 850°C, based on fitting to measured P concentration profiles.[143] The large supersaturation of self-interstitials, I, in region 2 arises from the presence of diffusing P-I pairs.

Figure 14. (a) High-resolution TEM showing SiP precipitate growth inward from the Si surface during P in-diffusion at 900°C.[146] The initial position of the Si surface is given by the dashed line. (b) Image showing $NiSi_2$ precipitation at a SiP particle during P-diffusion gettering.[146]

Figure 15. Model predictions of Fe gettering through $FeSi_2$ precipitation at SiO_2 sinks in the bulk of a wafer or by $FeSi_2$ precipitation at sinks on the back side of the wafer. The solution concentration at a depth of 1 μm is plotted as a function of anneal time. The thickness of the wafer is 0.5 mm, and a surface layer of thickness 10 μm is assumed to be free of gettering sinks.

Figure 16. Model prediction of Fe gettering by segregation to B-Si precipitates. The solution concentration at a depth of 1 μm is plotted as a function of anneal time. The B-Si particles are assumed to lie at a depth of 10 μm within the 0.5-mm wafer.

Figure 17. Model prediction of the time-dependent Fe concentration profile during segregation gettering by B-Si precipitates at 800°C. The B-Si particles are assumed to be clustered in a thin layer at a depth of 10 μm within the 0.5-mm wafer.

Figure 18. Model prediction of Fe gettering by substitutional B for the cases of epitaxial intrinsic Si on a B-doped substrate and an intrinsic-Si wafer containing a B-doped layer. The solution concentration at a depth of 1 μm is plotted as a function of anneal time. The thickness of the epitaxial Si layer and the depth of the 0.5-μm, B-doped layer are assumed to be 10 μm, with a total wafer thickness of 0.5 mm. The B concentration is 1×10^{19} atoms/cm^3 in both cases.

Figure 19. Theoretical modeling[139] of experimental results[20] for P-diffusion gettering of Au. A specimen initially containing a uniform Au concentration of ~3×10^{14} atoms/cm^3 was subjected to PDG at 988°C and then slowly cooled to 900°C followed by rapid cooling, yielding the depth profiles in (a). The sample was lastly annealed at 1150°C for 15 minutes, giving the final depth profiles in (b). Some theoretical parameters were adjusted to fit the P profiles.

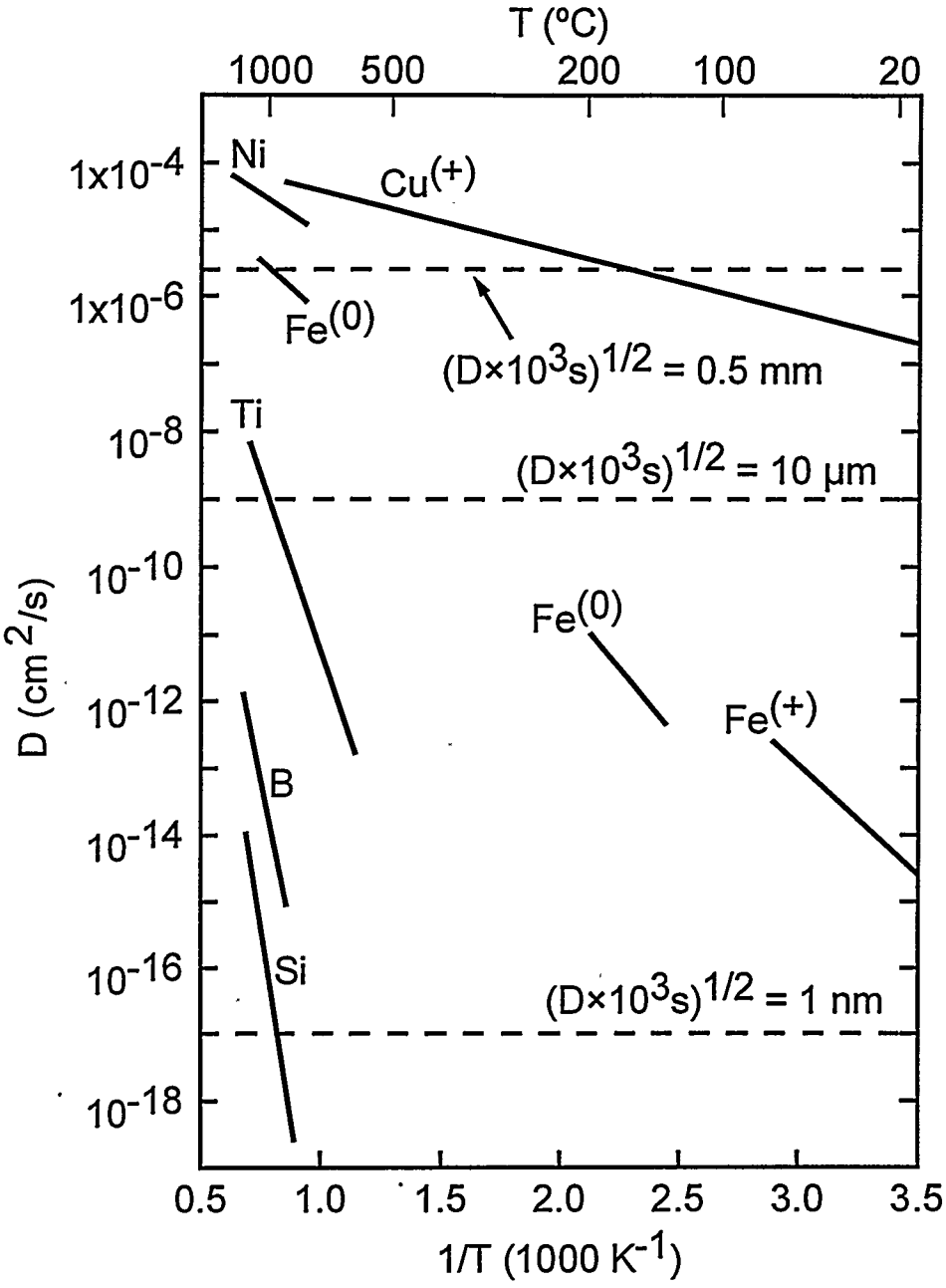

Figure 1. Diffusion coefficients of representative interstitial transition metals in Si, with charge state indicated where definitively known.[8,38-40] Included for comparison are the much smaller diffusion rates of two substitutional species, B and Si self-atoms. The horizontal dashed lines indicate approximate diffusivity thresholds for local atomic processes, proximity gettering, and back-side gettering.

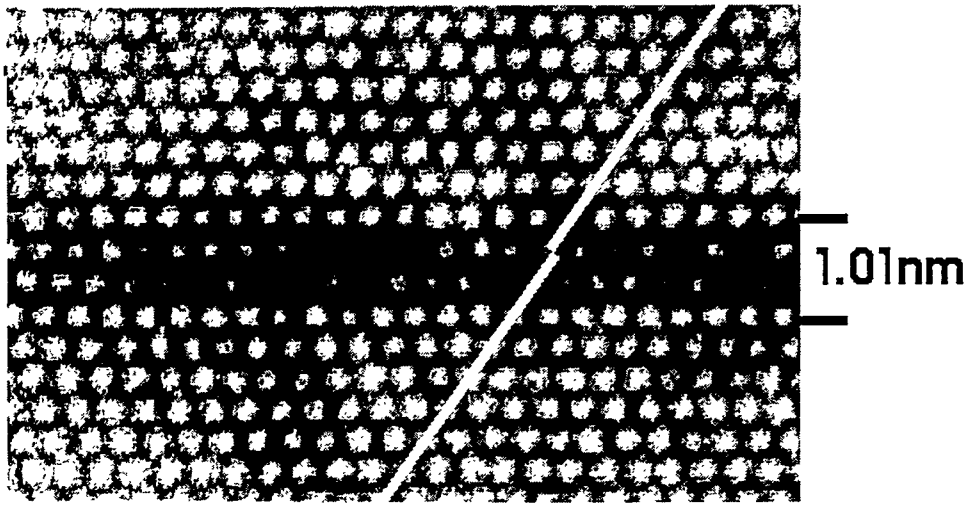

Figure 2. High-resolution TEM image of $NiSi_2$ platelet lying on $Si(1\bar{1}1)$ lattice planes after rapid quenching of a Si(Ni) solution from 1050°C.[45] The associated rigid shift of the Si lattice is indicated by the white line.

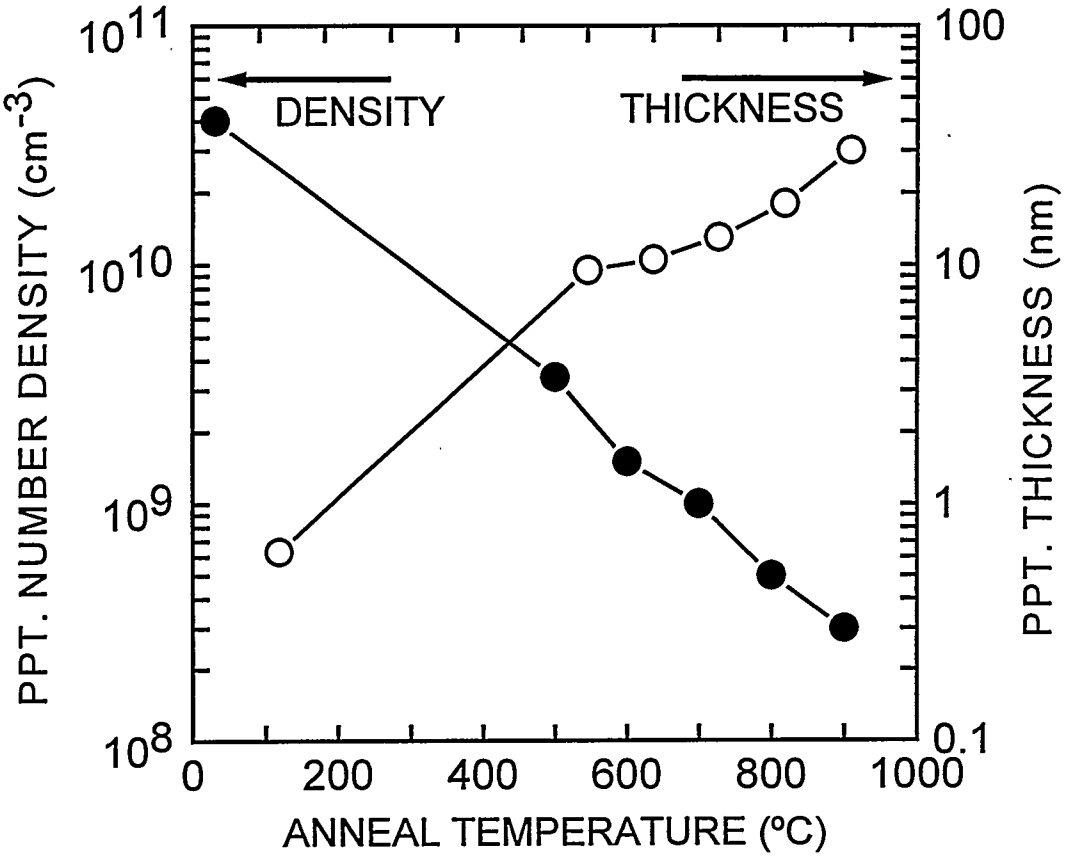

Figure 3. Ostwald ripening of $NiSi_2$ precipitates during annealing at various temperatures after quenching of a Si(Ni) solution from 1050°C.[45] The anneal time is 20 minutes.

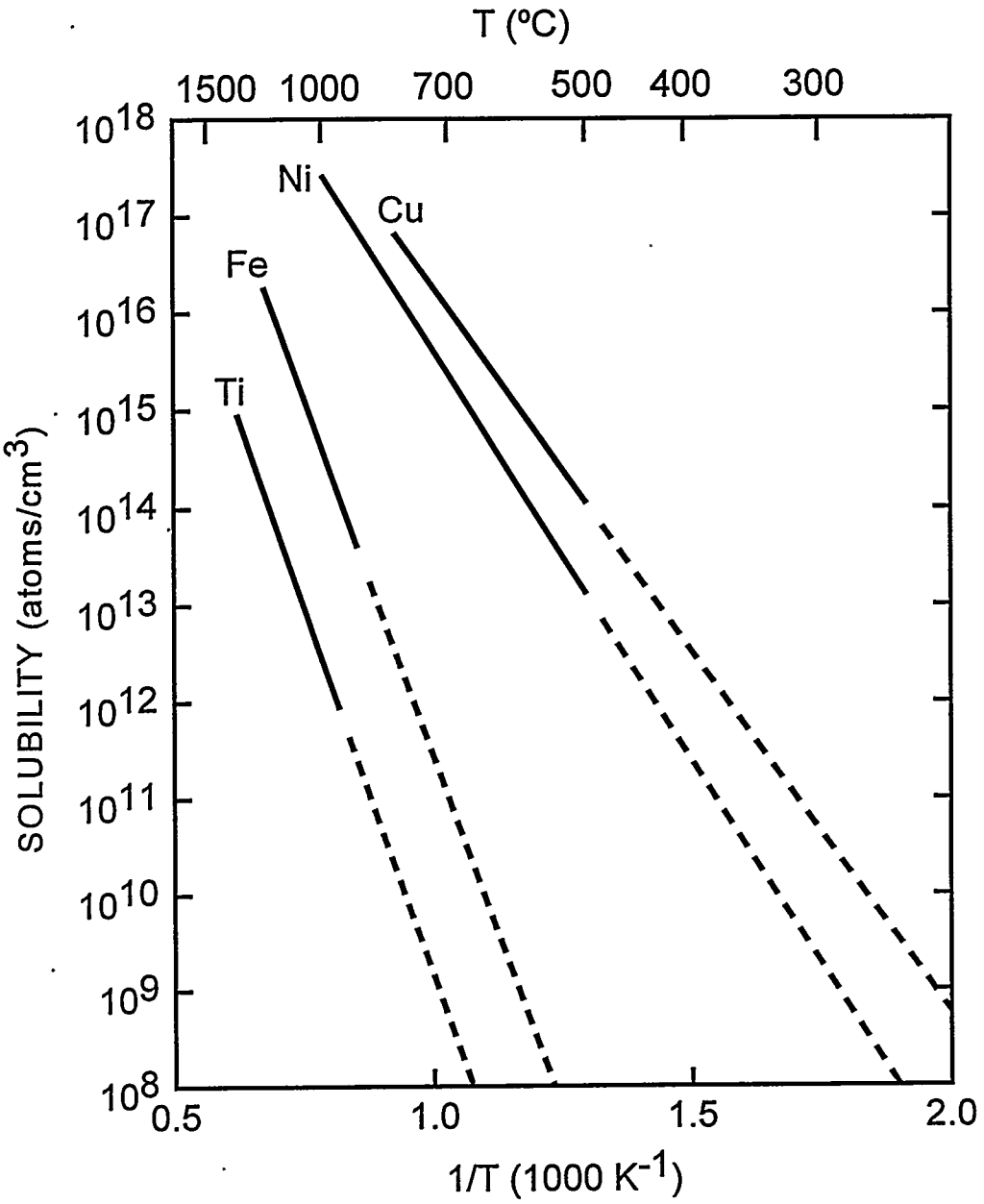

Figure 4. Solubilities of representative interstitial transition metals in Si below the eutectic temperature.[5,48] The solid lines show the range of experimental data, while the dashed lines are extrapolated.

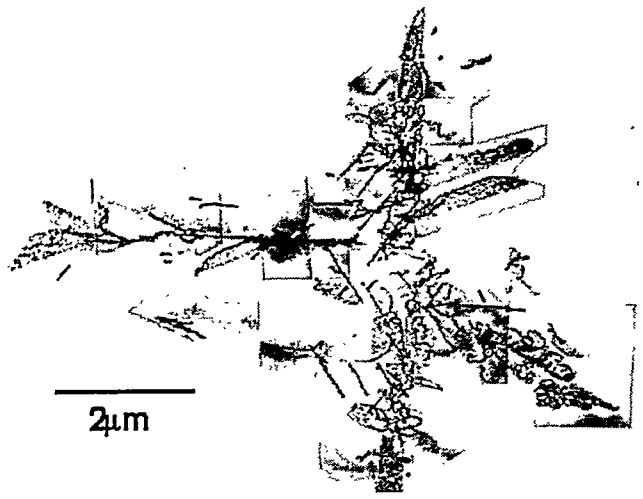

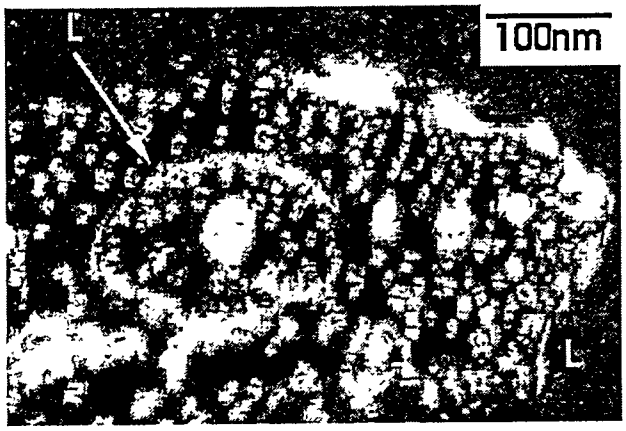

Figure 5. Colony of Cu_3Si precipitates in Si after cooling of a Si(Cu) solution from 900°C.[62] (a) Low-magnification TEM micrograph showing planar arrangements of dislocation loops and Cu_3Si precipitates. (b) Detail showing Moiré contrast at silicide particles.

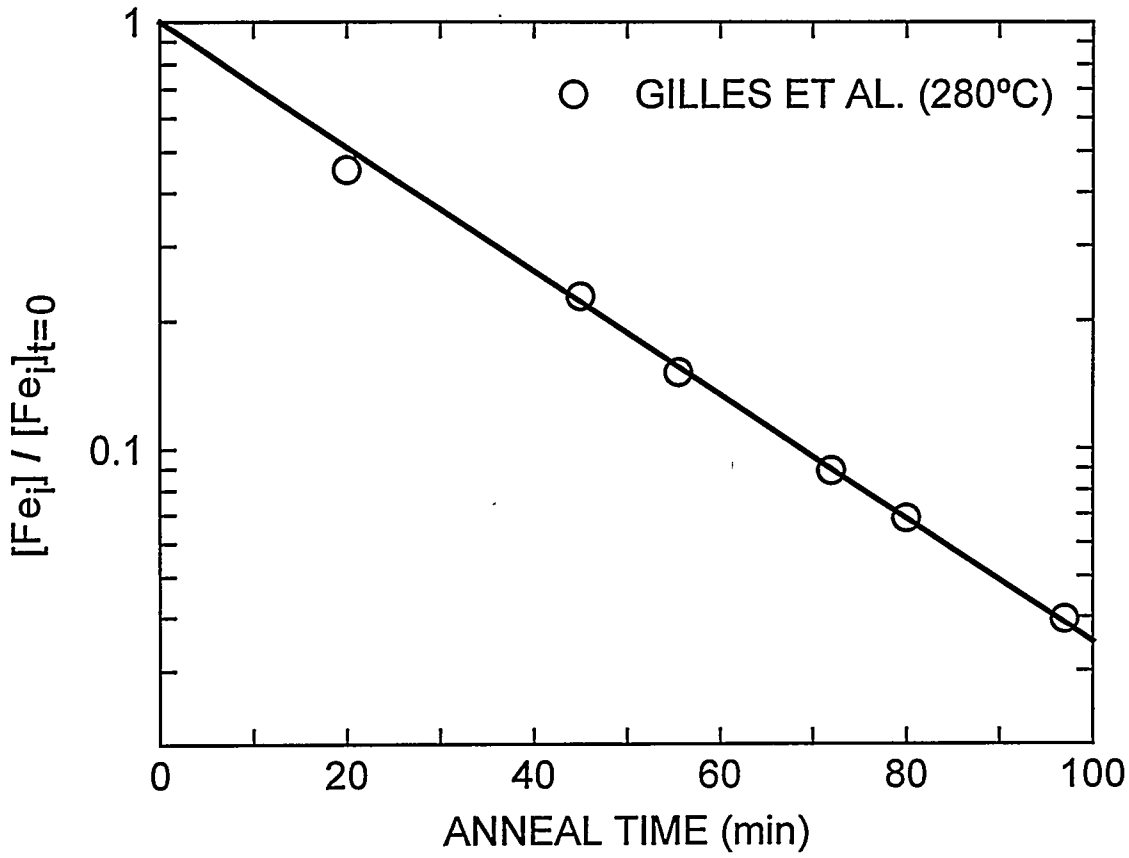

Figure 6. Reduction of Fe solution concentration due to $FeSi_2$ precipitation at SiO_2 particles at 280°C.[12] The initial Fe concentration is 7.2×10^{14} atoms/cm^3. The exponential decay is consistent with the diffusion-controlled kinetics represented by Eq. (6).

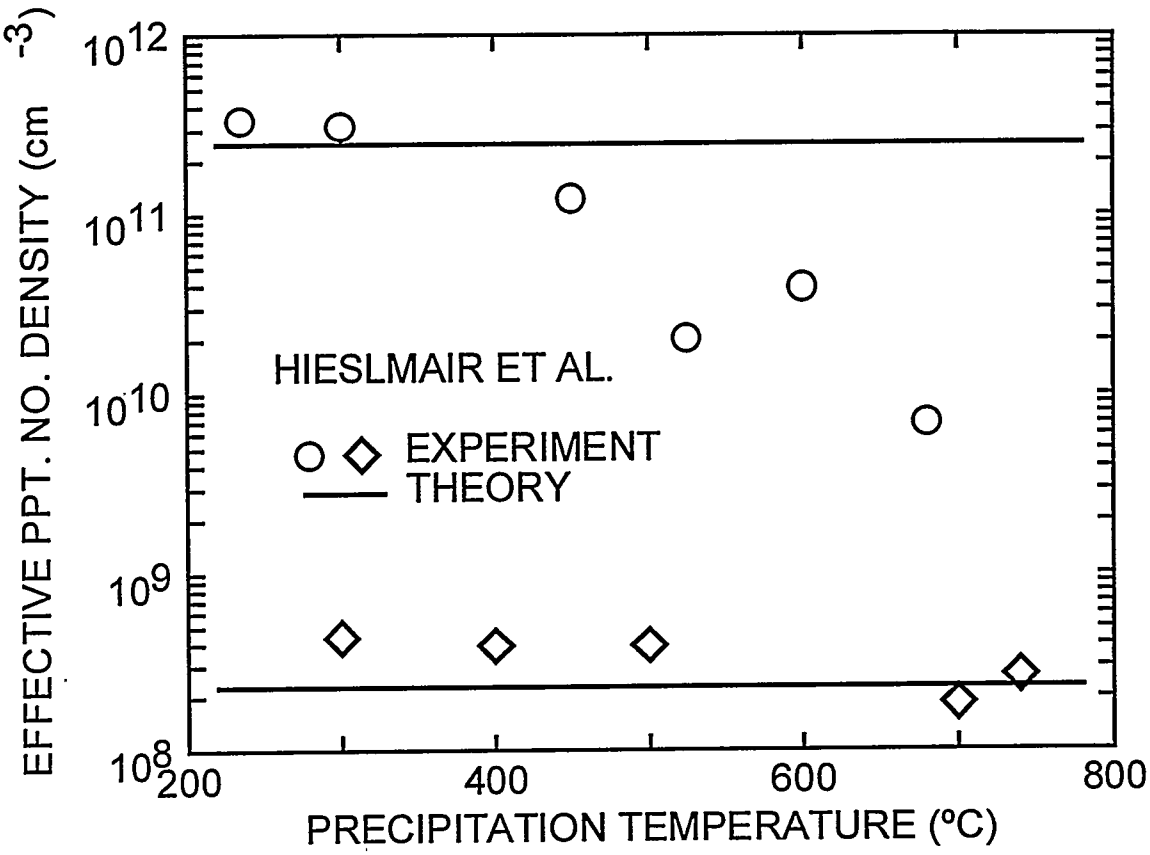

Figure 7. Effective density of SiO_2 sinks during $FeSi_2$ precipitation from solution for two SiO_2 densities and a range of temperatures, as derived by fitting of Eq. (6) to the experimentally measured decay of the Fe solution concentration.[13] The horizontal lines give the actual particle densities obtained from microscopy.

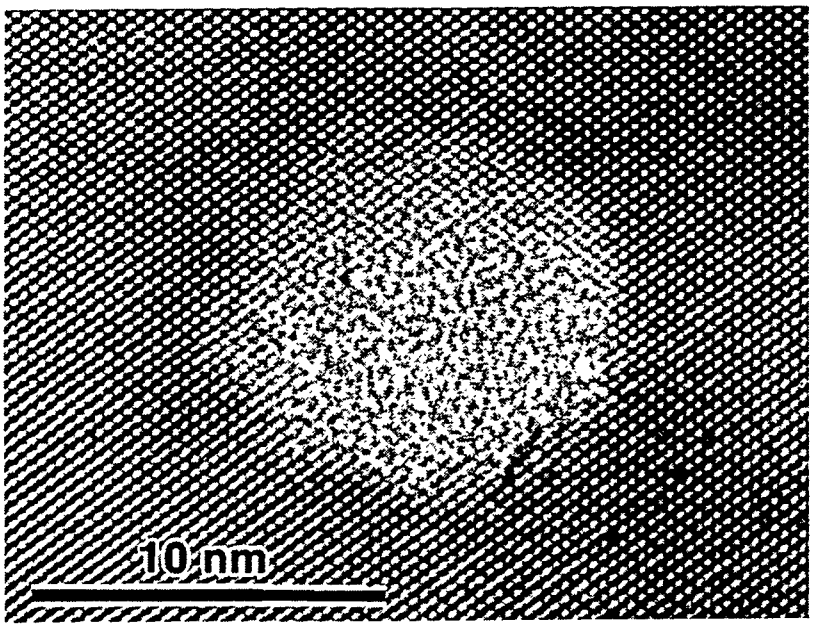

Figure 8. Phase-contrast TEM image of B-Si precipitate formed in Si by B ion implantation and subsequent annealing at 1100°C for 2 hours.[96] The pronounced, orientation-independent granularity of the particle image combined with the absence of an associated diffraction pattern are indicative of structural disorder.

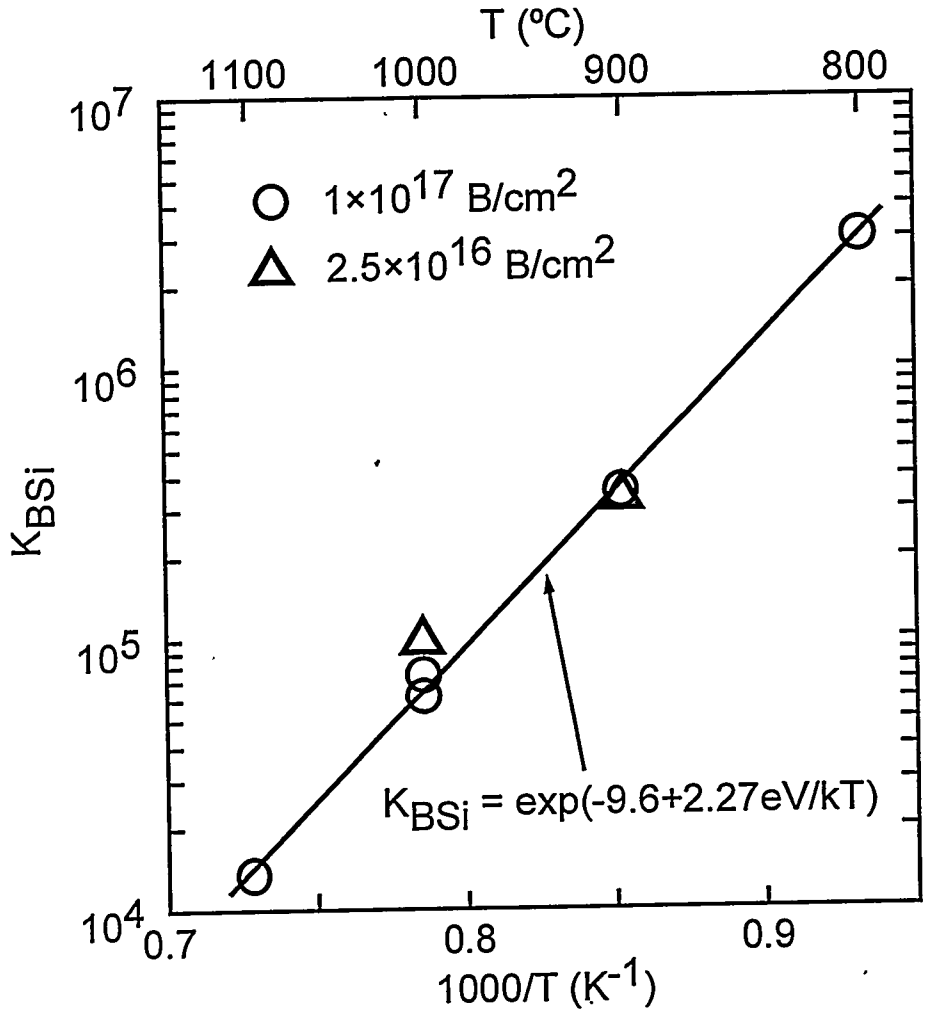

Figure 9. Segregation coefficient for gettering of Fe by B-Si precipitates.[24] The precipitates were formed by B ion implantation and annealing and then equilibrated with Fe in solution at a concentration equal to its solid solubility.

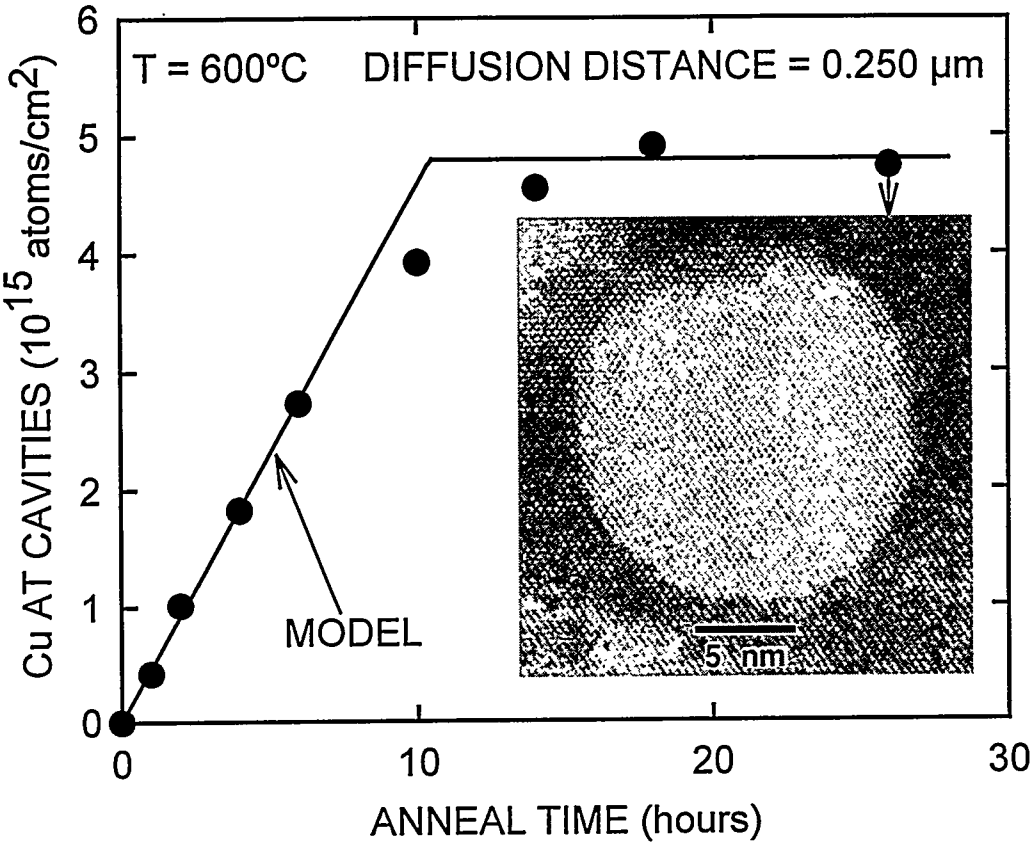

Figure 10. Redistribution of Cu from a layer containing Cu_3Si to a cavity layer on the opposite side of the Si wafer.[110] The line shows a fitted model calculation based on diffusion-limited flow to a strong, saturable sink. The high-resolution TEM image of a cavity after gettering shows no evidence of metal-silicide precipitation, consistent with gettering by a chemisorption trapping mechanism.

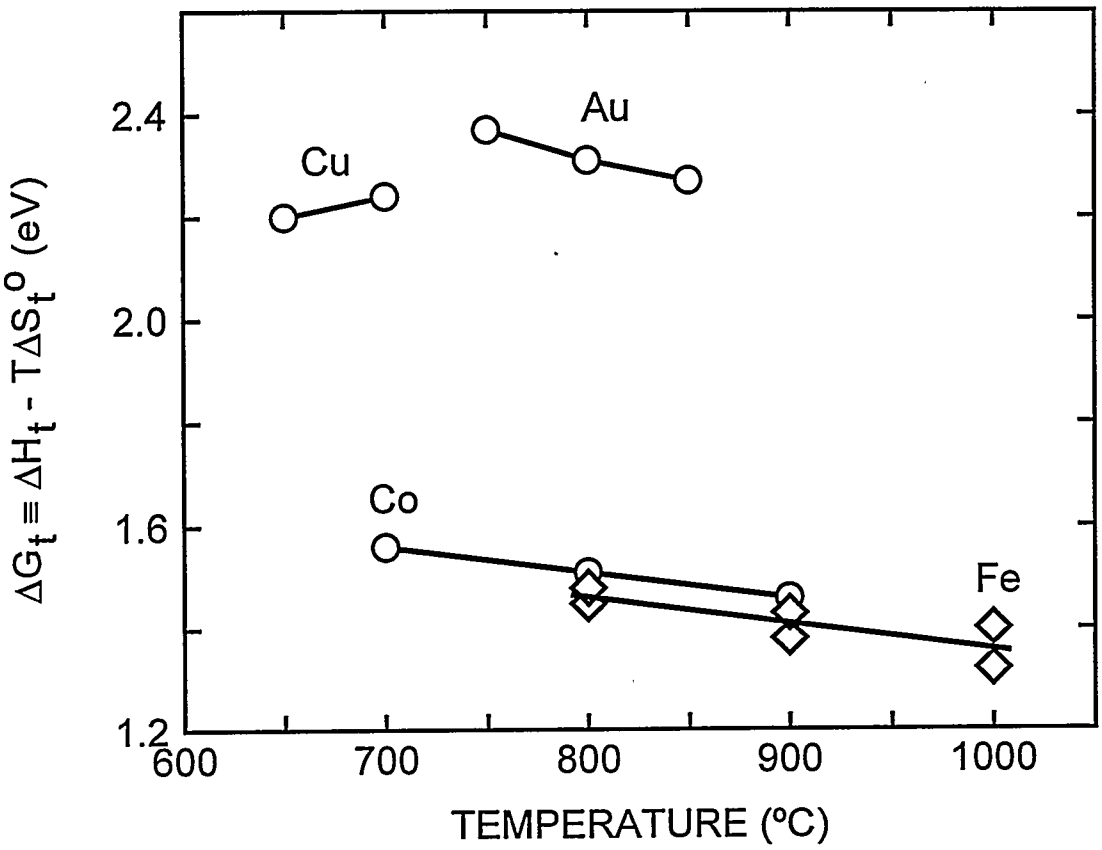

Figure 11. Binding free energies of transition metals at cavity walls obtained from application of Eqs. (9)-(11) to gettering experiments.[30,37,110]

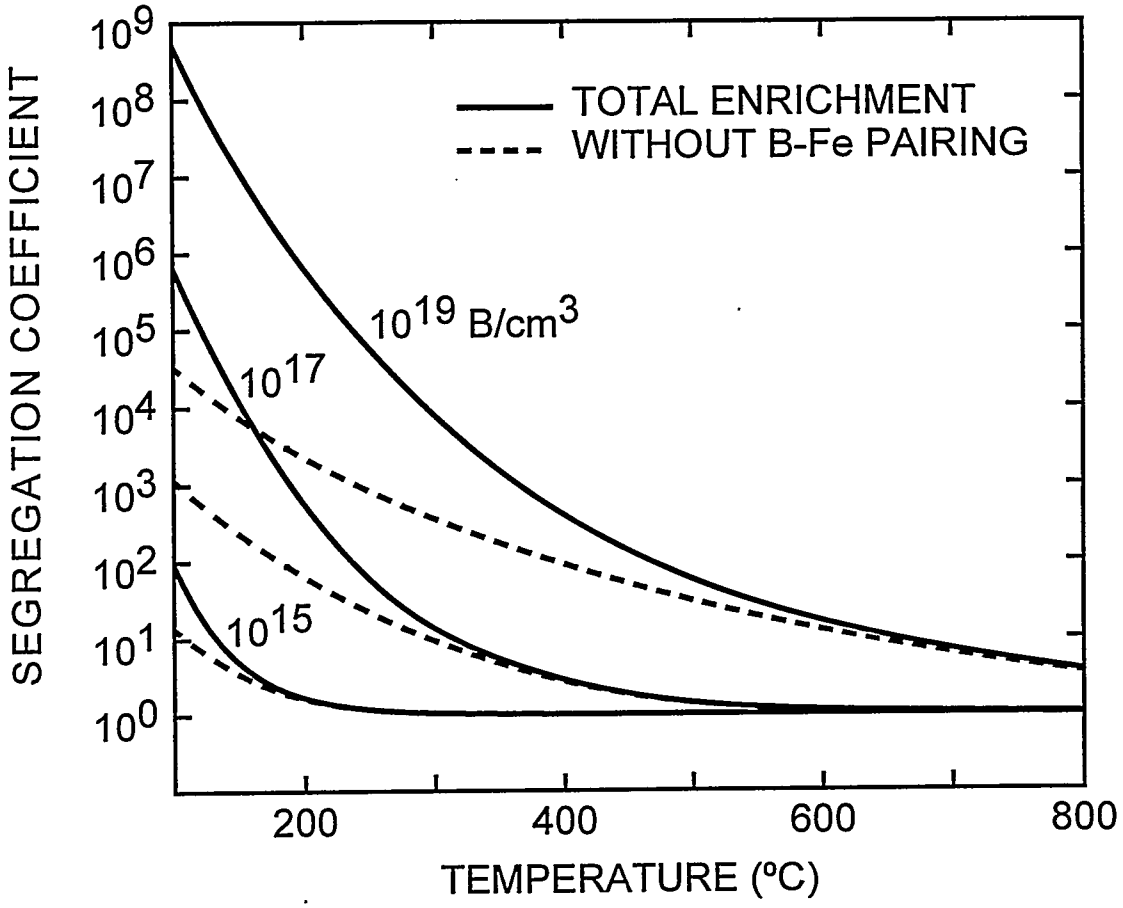

Figure 12. Predicted segregation coefficients for gettering of Fe in B-doped Si as a function of temperature and B concentration, obtained using Eqs. (12) and (13). The dashed curves show the effect of the dopant-induced Fermi-level shift alone, neglecting Fe-B pairing.

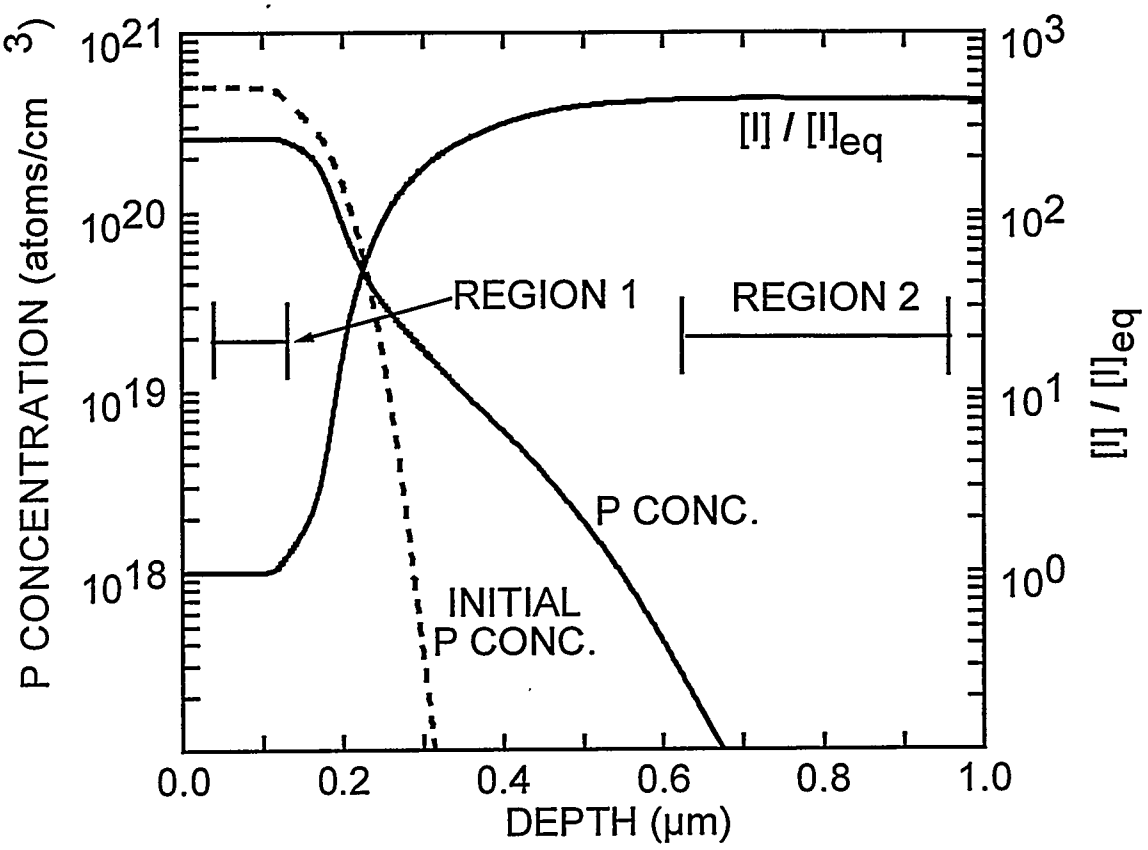

Figure 13. Theoretically calculated depth profiles associated with P diffusion at 850°C, based on fitting to measured P concentration profiles.[143] The large supersaturation of self-interstitials, I, in region 2 arises from the presence of diffusing P-I pairs.

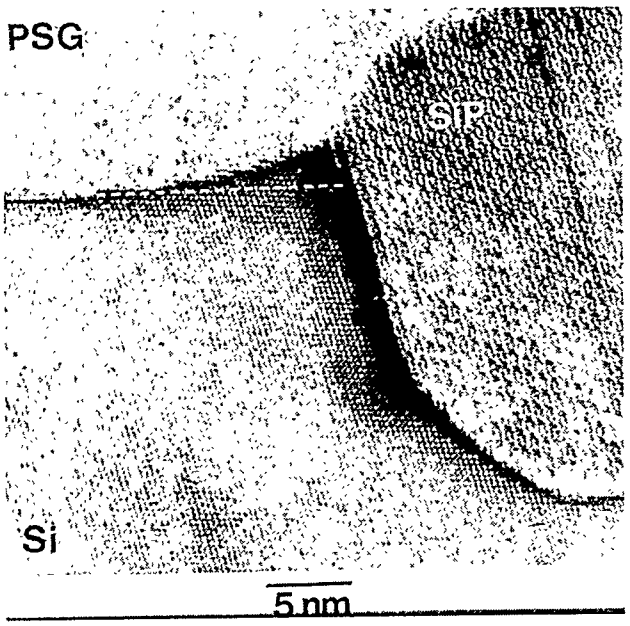

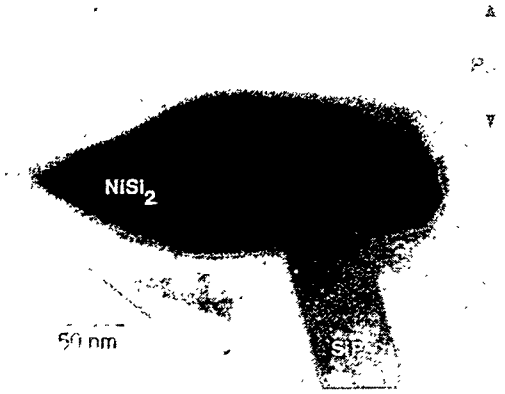

Figure 14. (a) High-resolution TEM showing SiP precipitate growth inward from the Si surface during P in-diffusion at 900°C.[146] The initial position of the Si surface is given by the dashed line. (b) Image showing $NiSi_2$ precipitation at a SiP particle during P-diffusion gettering.[146]

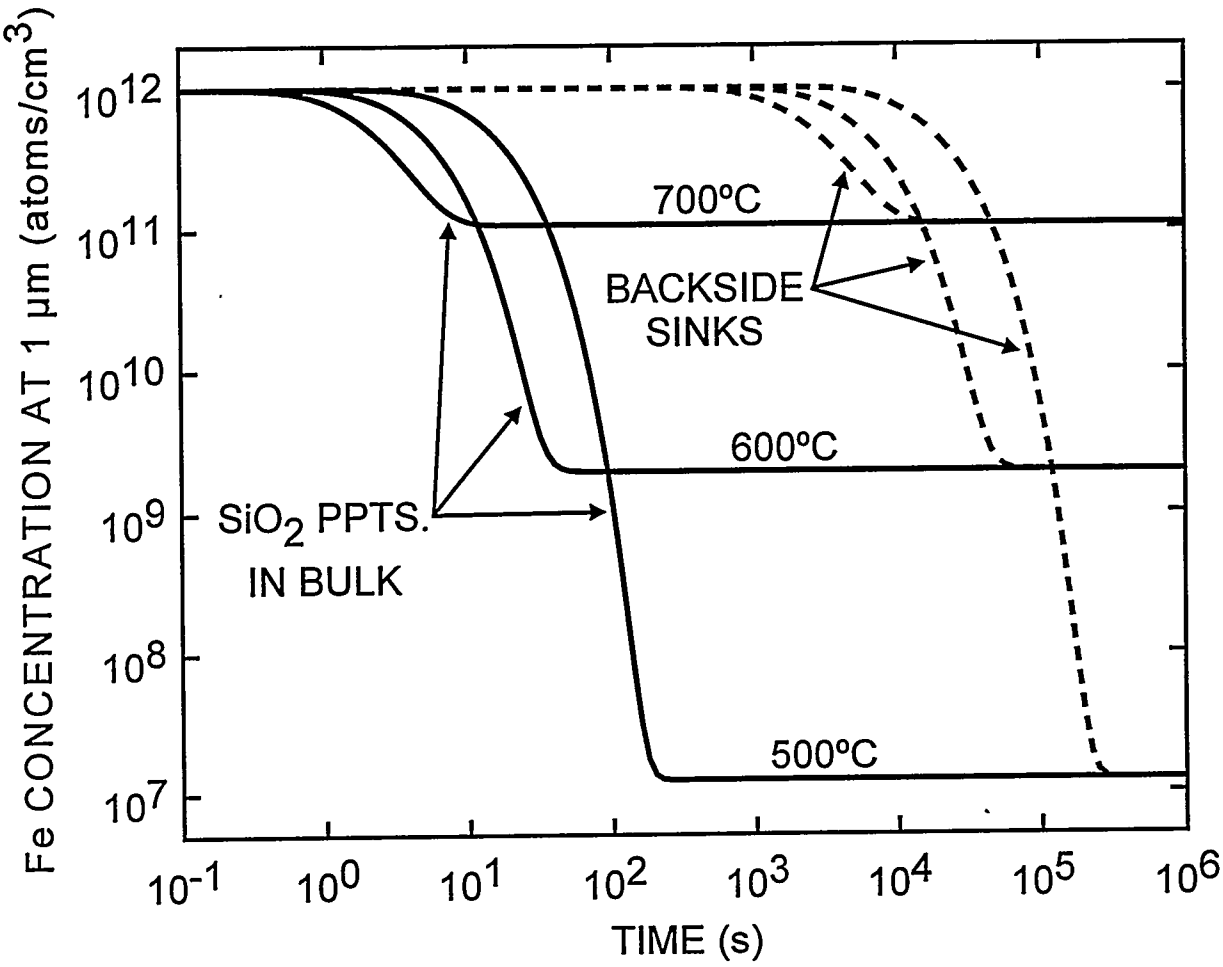

Figure 15. Model predictions of Fe gettering through $FeSi_2$ precipitation at SiO_2 sinks in the bulk of a wafer or by $FeSi_2$ precipitation at sinks on the back side of the wafer. The solution concentration at a depth of 1 μm is plotted as a function of anneal time. The thickness of the wafer is 0.5 mm, and a surface layer of thickness 10 μm is assumed to be free of gettering sinks.

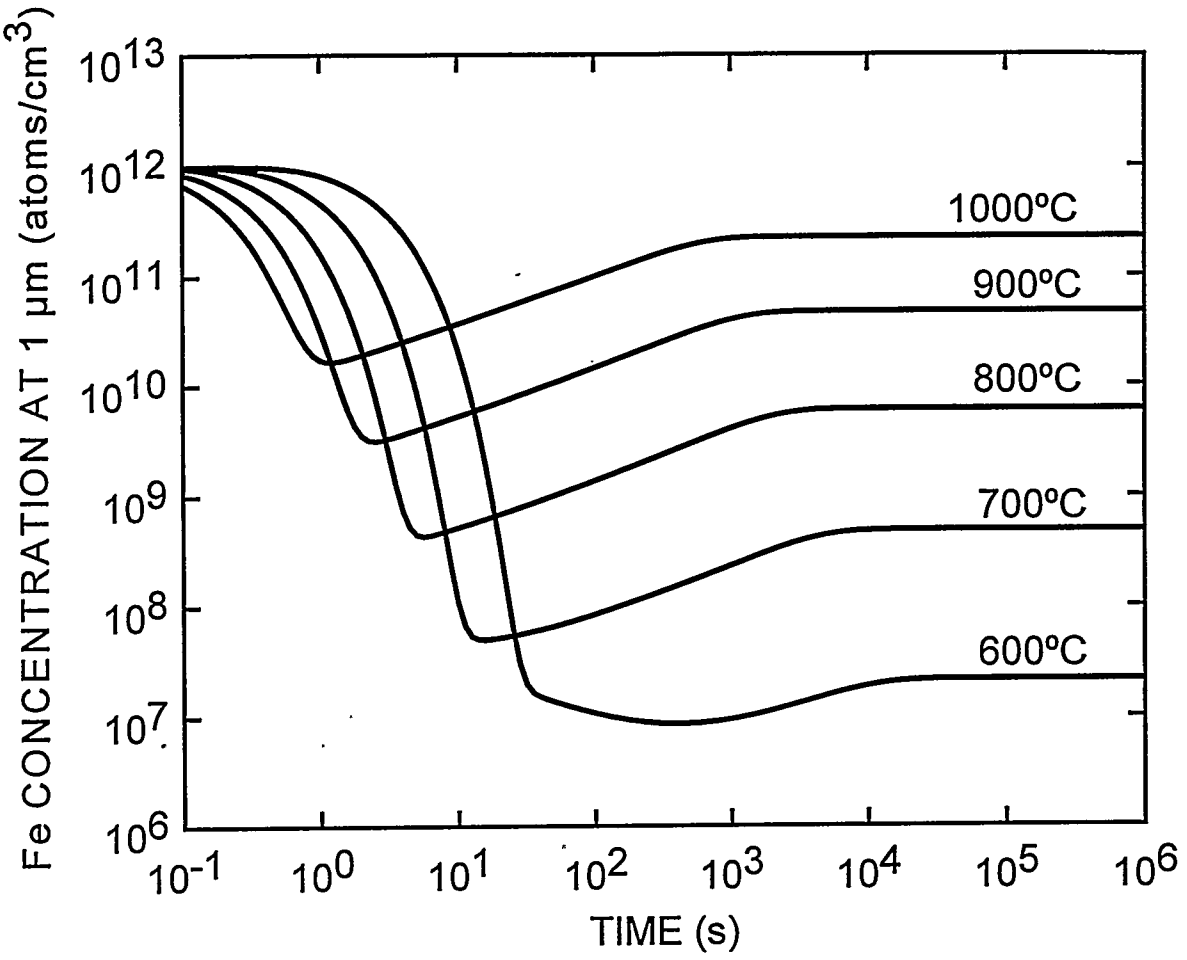

Figure 16. Model prediction of Fe gettering by segregation to B-Si precipitates. The solution concentration at a depth of 1 μm is plotted as a function of anneal time. The B-Si particles are assumed to lie at a depth of 10 μm within the 0.5-mm wafer.

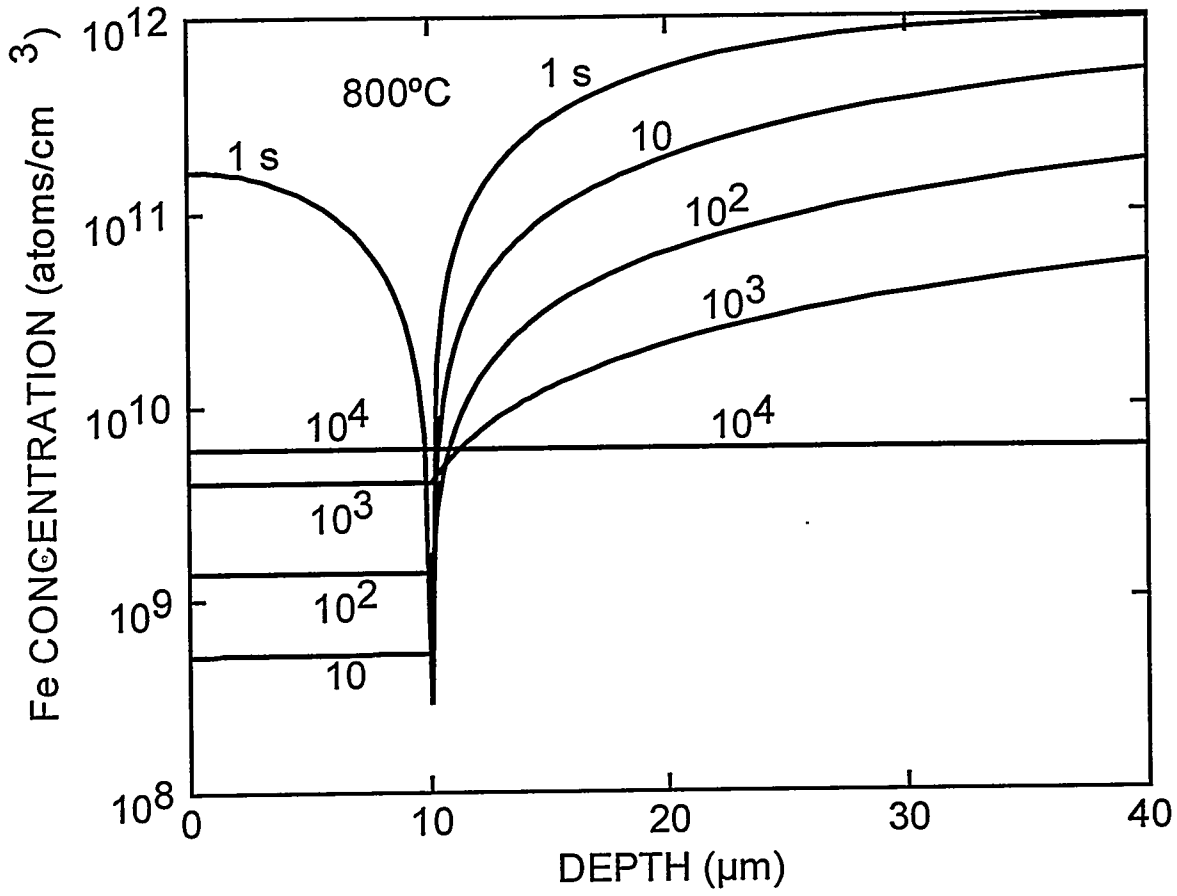

Figure 17. Model prediction of the time-dependent Fe concentration profile during segregation gettering by B-Si precipitates at 800°C. The B-Si particles are assumed to be clustered in a thin layer at a depth of 10 μm within the 0.5-mm wafer.

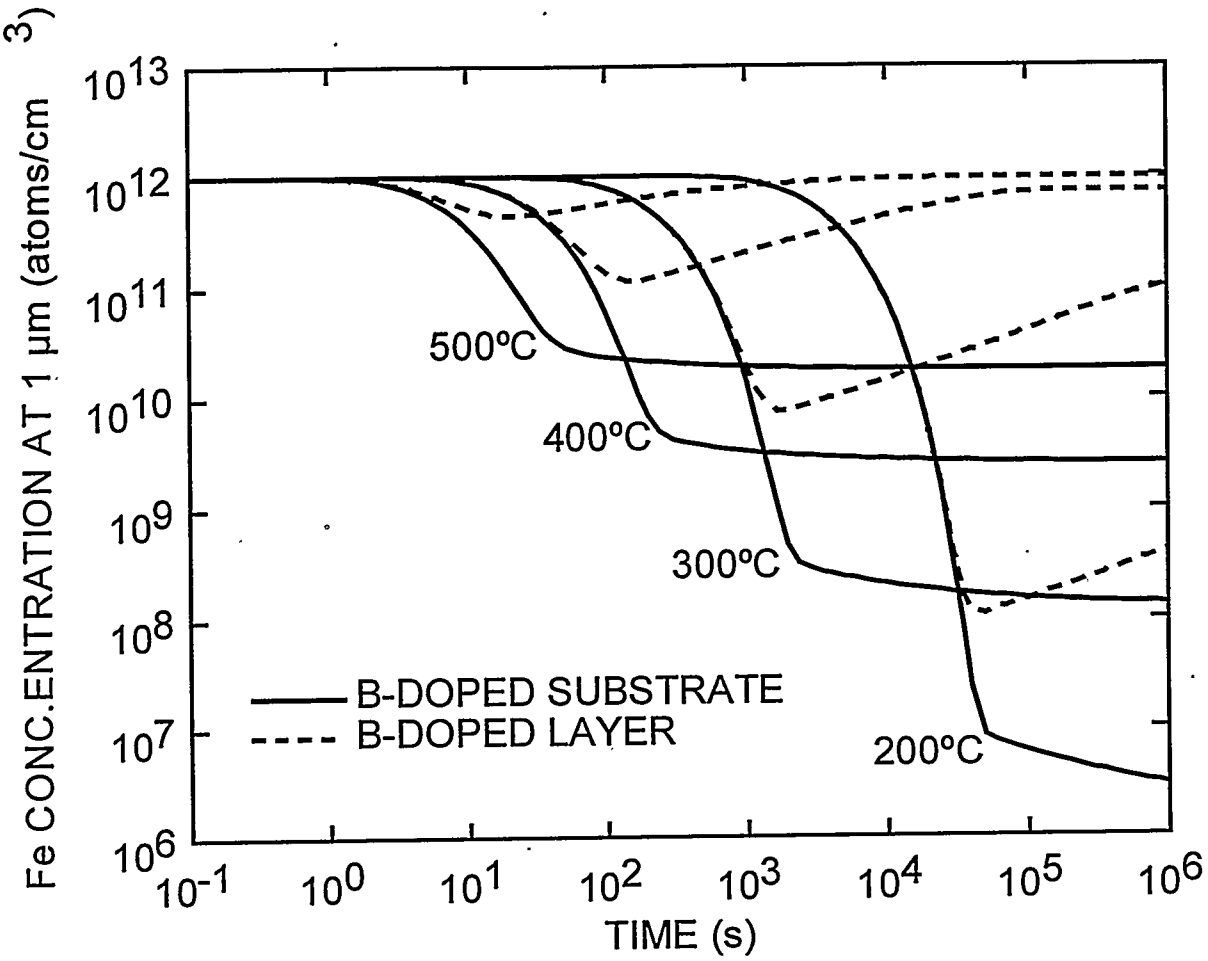

Figure 18. Model prediction of Fe gettering by substitutional B for the cases of epitaxial intrinsic Si on a B-doped substrate and an intrinsic-Si wafer containing a B-doped layer. The solution concentration at a depth of 1 μm is plotted as a function of anneal time. The thickness of the epitaxial Si layer and the depth of the 0.5-μm, B-doped layer are assumed to be 10 μm, with a total wafer thickness of 0.5 mm. The B concentration is 1×10^{19} atoms/cm^3 in both cases.

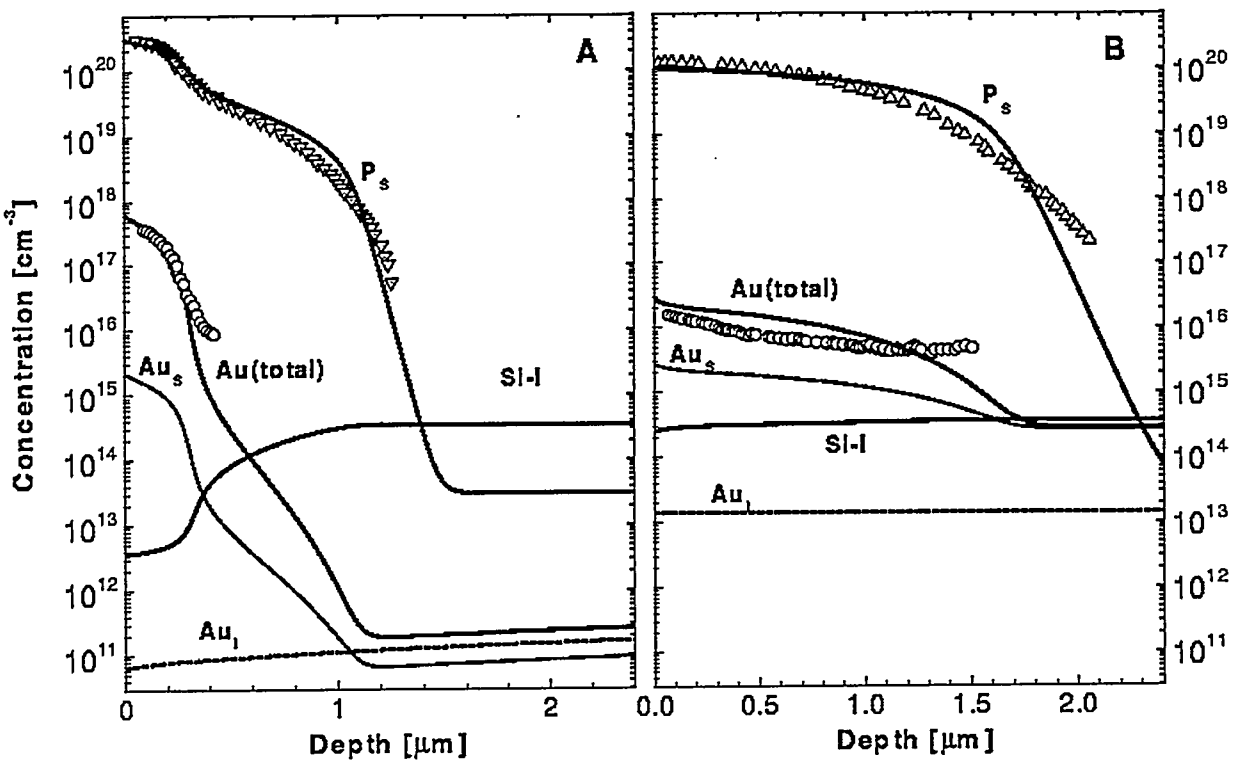

Figure 19. Theoretical modeling[139] of experimental results[20] for P-diffusion gettering of Au. A specimen initially containing a uniform Au concentration of ~3×10^{14} atoms/cm^3 was subjected to PDG at 988°C and then slowly cooled to 900°C followed by rapid cooling, yielding the depth profiles in (a). The sample was lastly annealed at 1150°C for 15 minutes, giving the final depth profiles in (b). Some theoretical parameters were adjusted to fit the P profiles.